Systematic computer-assisted proof of branches of stable elliptic periodic orbits and surrounding invariant tori

Daniel Wilczak[†§] and Roberto Barrio[‡¶]

Abstract. We present a concurrent algorithm for rigorous validation of the existence of continuous branches of stable elliptic fixed points for area preserving planar maps. The method utilises a classical theorem of Siegel and Moser combined with computed-assisted estimation of higher order derivatives of maps, continuation along the parameter range and concurrent scheduling of tasks.

We apply the algorithm to certain exemplary Poincaré maps coming from reversible or Hamiltonian systems: the periodically forced pendulum equations, the Michelson system and the Hénon-Heiles Hamiltonian. Moreover, our algorithm provides at once a Computer-Assisted Proof of the existence of wide branches of stable elliptic periodic solutions and the existence of invariant tori surrounding them.

Key words. stable elliptic periodic orbit, continuation, Computer-Assisted Proof, normal forms, invariant tori, resonances

AMS subject classifications. 65L07, 34D20, 68U20

1. Introduction.

It is well known from the work of Poincaré, that one of the first approaches in the theoretical and numerical analysis of dynamical systems is to compute and study the different invariant objects of the system, like periodic orbits, invariant tori, attractors and so on, that helps to the global study of the problem. For instance, qualitative properties of dynamical systems are often determined by periodic or quasi periodic motion. Also, hyperbolic periodic orbits give rise to chaotic dynamics provided their invariant manifolds intersect transversely. In parameterized families of maps there may occur various types of bifurcations influencing local or global dynamics of the system, like tangencies, period-doubling or cocoon bifurcations, just to mention few. And, for example, the study of the existence and stability or hyperbolicity of a particular periodic orbit is a quite routine task by means of computer assistance [4, 9, 10]. One just has to compute the derivative of a suitable Poincaré map at a periodic point and check whether its eigenvalues are not on the unit circle. Then one can conclude if the periodic orbit is a sink, saddle or source. We remark that hyperbolicity is a generic phenomenon, and thus, it is well suited for rigorous numerical methods. In fact, there are many efficient methods for validation not only the existence of periodic orbits but also for the computation of their invariant stable and unstable manifolds – see for instance [16, 17, 18, 19, 32].

Therefore, as one of the key information in a dynamical system, it is quite interesting to locate the position and stability of its periodic orbits [3, 20, 44]. Moreover, when the

[†]Faculty of Mathematics and Computer Science. Jagiellonian University. Łojasiewicza 6, 30-348 Kraków, Poland. (Daniel.Wilczak@ii.uj.edu.pl)

[‡]Departamento de Matemática Aplicada and IUMA. Computational Dynamics group. University of Zaragoza. E-50009. Spain. (rbarrio@unizar.es)

[§]Partially supported by the Polish National Science Center under Grant No. 2015/19/B/ST1/01454.

[¶]Partially supported by the Spanish Research project MTM2015-64095-P and by the European Social Fund and Diputación General de Aragón (Grant E48).

formulation of the problems has parameters, such as the energy, the dependence in terms of them provides a global information of the parametric changes of the system [5, 6, 11, 12]. In particular, if we have a periodic orbit and we vary the value of a parameter, the initial conditions of the periodic orbit change, following a path generating a whole family of periodic orbits, whose plot describes some aspects of the system. These families of periodic orbits are usually obtained numerically using different approaches in literature [4, 22, 23, 27, 48, 49, 50], and just in very few cases it is possible to give an analytical expression or proof. In Hamiltonian systems periodic orbits usually appear in families parameterized by the total energy. In this case the verification of stability of a periodic orbit is more complicated. Since the system is measure preserving, the product of all Floquet multipliers of a periodic orbit is always equal to 1. Even if all of them are on the unit circle the orbit may be unstable due to the so called Arnold diffusion [2]. Therefore, linearization at a periodic orbit does not give sufficient information about its stability and higher order terms must be analysed.

The aim of this paper is to provide an algorithm for validation of the existence and stability of branches of elliptic fixed points for a one-parameter family $f : P \times \mathbb{R}^2 \to \mathbb{R}^2$ of an analytic area preserving or reversible map. In this case, due to the classical analytical result by Siegel and Moser [46], an elliptic (and symmetric in reversible settings) fixed point is generically surrounded by invariant curves provided no strong resonances are present. These invariant curves separate the phase space. The domain surrounded by such a curve (that contains the fixed point) is mapped into itself and thus the fixed point is stable.

The method proposed in this paper utilises the above famous KAM theorem of Siegel and Moser [46] with rigorous computer-assisted estimations of higher order derivatives of the map under consideration. By rigorous computation we mean computation performed using interval arithmetics [42] that gives guaranteed bounds on computed quantities, and therefore it allows to state theorems.

After reduction to a carefully chosen Poincaré map the proposed algorithm applies to two degrees of freedom (2DOF) Hamiltonian systems (4D systems), 2D non-autonomous Hamiltonian systems and 3D reversible ODEs. In the 4D Hamiltonian case a Poincaré map can be seen as a family of independent area preserving maps parameterized by the total energy. In non-autonomous 2D Hamiltonian case we may impose T-periodicity in time and then the method applies to the map defined as a time T shift along trajectories. The result by Siegel and Moser [46] applies also to symmetric fixed points of reversible planar maps. If the Poincaré section of a reversible system is self-symmetric, then the associated Poincaré map is reversible too, and the algorithm applies.

Recently, different research groups have just proposed algorithms for validated computation of invariant tori [28, 29, 33]. In the papers [28, 29], the authors solve associated invariance equation for the parameterization. Thus, their method gives not only the existence, but also quantitative estimates on an invariant torus. The authors present an application of the proposed approach to several explicitly given maps. Although it seems that the above method could be applied to invariant tori near elliptic periodic orbits for ODEs, either by reduction to a Poincaré map or by time-space parameterization of an invariant torus, such an application is not provided.

The method proposed in the present paper is a two-dimensional optimized version of a general case just proposed in [33]. In both papers, the existence of a family of invariant tori

is obtained by checking that the assumptions of the KAM theorem are satisfied (that is, the natural way used in KAM literature). Although the nice paper [33] provides a methodology for computer-assisted validation of KAM tori near an elliptic periodic orbit in a higher dimensional system (exemplary in some particular important periodic orbits), no systematic algorithmic approach is given as most of the parameters of the validation algorithm have been adjusted by hand. In contrast, the present paper focuses on the systematic validation of long branches of stable elliptic periodic orbits, and not only around particular ones. In this case, the parameters of the validation routine (like the parameter range, predicted enclosure for branch of elliptic orbits) must be adjusted automatically. This requires some algorithmic effort to make computation of long branches of elliptic orbits surrounded by tori possible in a reasonable CPU time. Moreover, our algorithm detects automatically strong resonances, changes in the twist direction and gives explicit bounds on the parameter range where they appear. In consequence, a quantitative estimate on the stability range in the parameter space of the system is computed.

We would like to emphasise that the application of the method to ODEs, and not directly to a map, requires an efficient algorithm that rigorously computes higher order derivatives of Poincaré maps. For this purpose we used the $\mathcal{C}^r$-Lohner algorithm [56].

In real computation it is very unusual that we can validate the existence of a branch of elliptic periodic orbits $u : P \to \mathbb{R}^2$ for wide range of parameters P without subdivision of P. Close to the resonances the number of necessary subdivisions may be huge. In this context another (very technical but important) issue arises that is behind the main validation algorithm: concurrent (or parallel) scheduling of subdivisions of the range of parameter values P into many processors. We would like to emphasise that uniform or binary subdivisions (as in many branch-and-bound algorithms) are extremely inefficient in this case. Since we deal with a continuous object (a branch of periodic orbits) the parameters of the validation algorithm should continuously depend on the parameter of the map under consideration. Some aspects concerning adaptivity and concurrency in the algorithms will be discussed in Section 3 and Section 4.

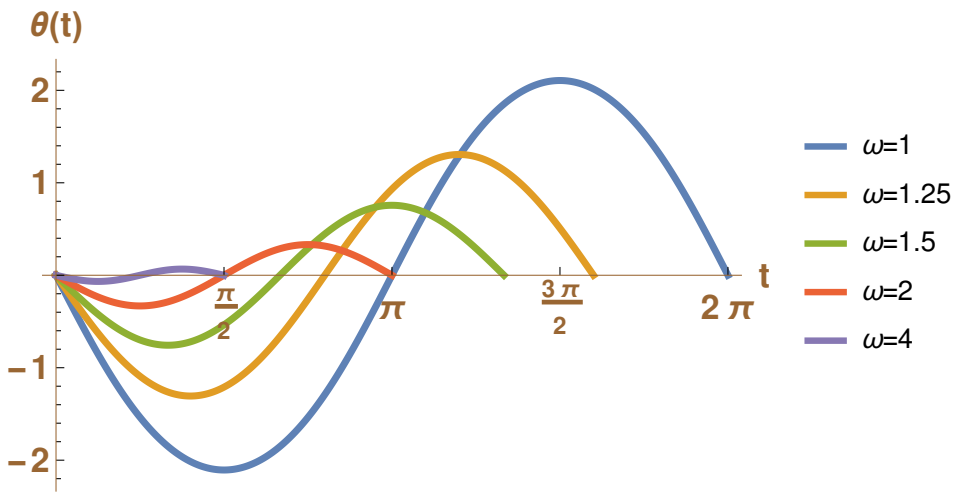

Figure 1. *Odd elliptic periodic solutions of the system ((2)) for selected parameter values ω.*

In order to justify applicability of the proposed method we present in this paper a Computer-Assisted Proof of the existence and stability of elliptic periodic orbits and invariant tori for three ODEs: a periodically forced pendulum (2D non-autonomous Hamiltonian system), the Michelson system [41] (3D reversible system) and the well known Hénon-Heiles Hamiltonian (4D autonomous Hamiltonian system). For instance, the algorithm we propose applied to the periodically forced pendulum system yields to the following rigorous result:

Theorem 1.1. *For all parameter values* $\omega \in \overline{\Omega \setminus (G_1 \cup G_2 \cup G_3 \cup G_4)}$, *where* $\Omega \equiv [1, 31]$ *and*

$$\begin{aligned} G_4 &\equiv 3.997772676398^{706266}_{326566} && \textit{(1:4 resonance)} \\ G_3 &\equiv 2.9940916840^{28588500}_{12414777} && \textit{(1:3 resonance)} \\ G_2 &\equiv 1.970242^{591584483455}_{101046491000} && \textit{(1:2 resonance)} \\ G_1 &\equiv 1.018227^{823641081788}_{398927290977} && \textit{(1:2 resonance)} \end{aligned} \tag{1}$$

the Poincaré map of the periodically forced pendulum equation

$$\ddot{\theta} = -\sin(\theta) + \sin(\omega t), \tag{2}$$

defined as a $2\pi/\omega$ *shift along the solutions, admits an elliptic fixed point* $(0, \dot{\theta}_\omega)$. *Moreover, any neighbourhood of this fixed point contains an invariant curve (for the Poincaré map) surrounding the fixed point. The corresponding solution* $\theta_\omega(t)$ *to the system* (2) *with the initial condition* $(\theta(0), \dot{\theta}(0)) = (0, \dot{\theta}_\omega)$ *is an odd* $2\pi/\omega$*-periodic function.*

Note that this theorem provides "de facto" a proof of the existence of the continuous family of elliptic fixed points, but also the existence of surrounding invariant tori. On Figure 1 we show odd periodic solutions resulting from Theorem 1.1 for selected parameter values. There is a numerical evidence that this family of odd periodic solutions continues to exist when $\omega \to \infty$.

Our algorithm automatically detects approximate parameter values for which bifurcations or resonances may occur. Since the exact value of a resonant parameter is usually unknown, our rigorous routine must exclude a tiny gap around it. The four gaps G_1, G_2, G_3 and G_4 listed in (1) correspond to *strong resonances* (see Subsection 2.4). On Figure 2, two phase portraits of the Poincaré map P_ω are shown for parameter values close to 1:3 and 1:2 resonances.

This paper is organized as follows. In Section 2 we present the rigorous numerical algorithms that verify the existence and stability of an elliptic fixed point. In Section 3 and Section 4 we focus on some technical details on the computer implementation of several improvements of the algorithms introduced in Section 2. As important applications of the tools, in Section 5, Section 6 and Section 7, we present new theorems obtained with the help of the algorithms developed in the previous sections for the perturbed pendulum, the Michelson system and the Hénon-Heiles Hamiltonian, respectively. Details of the formulae of the Birkhoff normal form are given in the Appendix. Finally, we present some conclusions.

1.1. Notation. In the subsequent algorithms by *interval vector* $[v]$ we mean a subset of $\mathbb{R}^n$ which is a Cartesian product of closed intervals. An *interval matrix* $[A]$ is a subset of $\mathbb{R}^{n\times n}$ such that all entries of the matrix are closed intervals. By I we will denote the $n \times n$ identity matrix. By *interval hull* of a set $B \subset \mathbb{R}^n$ (denoted by $\square B$) we mean the smallest interval vector (in the sense of inclusion) that contains B.

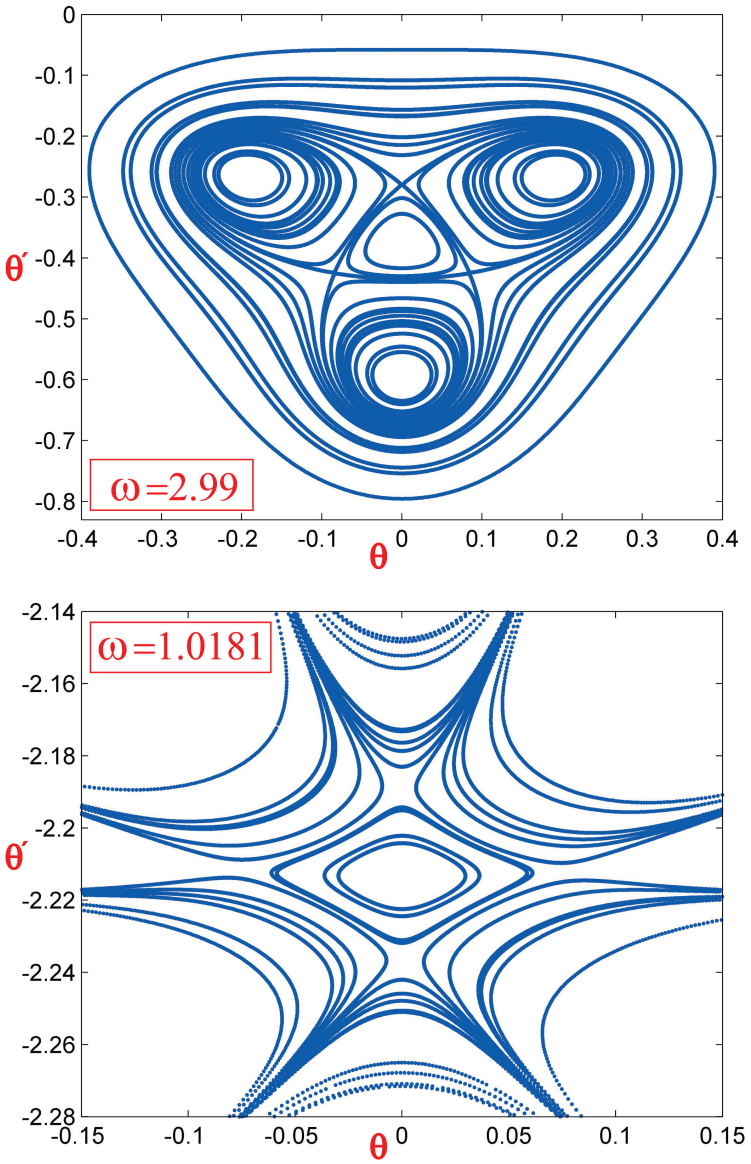

Figure 2. *Phase portrait of the Poincaré map P_ω for the system (2) in a neighbourhood of an elliptic periodic orbit for two parameter values ω near to 1:3 (top) and 1:2 (bottom) resonances.*

2. The Algorithm: existence and stability of an elliptic fixed point of an area preserving map. In this section we will give more details of the main steps of the algorithm that verifies the existence and stability of an elliptic fixed point of an area preserving map f_p depending on one parameter p. The algorithm consists of the following steps that will be described in detail in the sequel.

1. For a given parameter value p, we find a good numerical candidate for a fixed or

periodic point of the map f_p. This step may be performed (for instance) by the classical Newton method applied to f_p with continuation along the branch of parameters $p \in P$.
2. We validate (when possible) the existence of a family $P \ni p \to x_p \in N$ of periodic orbits, where N is a computable bound on the range of the curve. Here we are using the Interval Newton method [1, 42, 43].
3. We compute (when possible) the Birkhoff normal form [13] of the map f_p at x_p for all $p \in P$ up to certain order.
4. If the previous steps (Steps 2 and 3) succeed, we check the twist condition [46] that guaranties the stability of the orbits (`Success`).
5. If one of the above steps fails, we rearrange the parameters of the method (like the size of parameter range P, size of the set N) and we try to repeat the computations until we succeed or until we reach some threshold values of parameters which indicate that the program should stop further subdivisions (`Fail`).

If the algorithm returns `Success`, then the Computer-Assisted Proof technique (CAP) has managed to give a *rigorous proof of the existence of an elliptic fixed point and surrounding invariant tori* for all parameter values $p \in P$. In the next subsections we describe in some detail all the steps and the required theoretical results.

2.1. The validation of the existence of branches of fixed points. There are many methods for the validation of the existence of fixed points by means of computer assistance. Some of them are topological (like the Conley index, shooting method, Brouwer theorem). Other methods, and in particular some of the most efficient methods for proving the existence and uniqueness of zeros of smooth maps, are based on the direct use of the Interval Newton method [1, 8, 9, 10, 42, 43], and it gives our Algorithm 1 (`proveFixPointBranch`) below.

Let $f : P \times \mathbb{R}^2 \to \mathbb{R}^2$ be a map under consideration, i.e. we assume that for $p \in P$ the mapping $f_p := f(p, \cdot)$ is analytic and area preserving on some domain. Our first step is to verify that there is a smooth branch $P \ni p \to x_p \in \mathbb{R}^2$ of isolated fixed points for f_p.

The following lemma, that provides the theoretical properties of Algorithm 1, is a direct consequence [1, 8, 9, 10, 42, 43] of the properties of the Interval Newton Operator and the implicit function theorem.

Lemma 2.1. *Assume Algorithm 1 is called with its arguments $(P, f, [X])$ and let $[N]$ be the result of the algorithm. If $[N] \neq \emptyset$, then for all $p \in P$ the mapping $f_p := f(p, \cdot)$ has a unique fixed point $x_p \in [N]$. Moreover, the function $p \to x_p$ is of class $\mathcal{C}^1$.*

That is, in the Algorithm 1, when the return is $[N] \neq \emptyset$, what we have is the interval vector where a smooth branch of isolated fixed points x_p for f_p exists, and so the result of the CAP is `Success`. In case of return $\emptyset$, it means that more refinements are required (`Fail`).

2.2. Birkhoff normal form of area preserving maps. The second step of our main algorithm is the computation of the Birkhoff normal form of an analytic area preserving map. The routine is straightforward and it is based on the implementation of an explicit formulae which will be given in the Appendix A. Here we shortly recall what the Birkhoff normal form is, and we impose that there is a routine that computes such representation of a map.

Definition 2.2. *Let $f : \mathbb{R}^2 \to \mathbb{R}^2$ be a smooth area preserving map, and let $x \in \mathbb{R}^2$ such that $f(x) = x$ (a fixed point). Let λ_1 and λ_2 be the eigenvalues of $Df(x)$. Following [46] we will*

Algorithm 1 `proveFixPointBranch`

Input:
$P \subset \mathbb{R}$: interval of parameters,
$f : P \times \mathbb{R}^2 \to \mathbb{R}^2$: $\mathcal{C}^1$ mapping,
$[X] = [a, b] \times [c, d] \subset \mathbb{R}^2$: an interval vector in which we expect the existence of an unique curve $p \to x_p$ solving $f(p, x_p) \equiv x_p$, for $p \in P$.

Output: $[N]$: subset of $\mathbb{R}^2$

$x_0 \leftarrow \{\frac{1}{2}(a + c, b + d)\}$ ▷ center of $[X]$
$[A] \leftarrow \square\{D_x f(P, [X])\}$ ▷ take interval hull of the set of derivatives
if $[A] - I$ is not invertible **then**
  return $\emptyset$
end if
$[N] \leftarrow x_0 - ([A] - I)^{-1} \cdot (f(P, x_0) - x_0)$ ▷ Interval Newton operator
if $[N] \not\subset \mathrm{int}([X])$ **then**
  return $\emptyset$
end if
return $[N]$

call the point x

- hyperbolic *if* $\lambda_1, \lambda_2 \in \mathbb{R}$ *and* $\lambda_1 \neq \lambda_2$,
- elliptic *if* $\lambda_1 = \overline{\lambda_2} \in \mathbb{C} \backslash \mathbb{R}$ *and* $\lambda_1 \neq \lambda_2$,
- parabolic *if* $\lambda_1 = \lambda_2$.

The next theorem and its proof tell how to bring a planar area preserving map in a neighbourhood of an elliptic fixed point into the form Theorem 2.3.

Theorem 2.3. *[46, §23] Consider an analytic area preserving map* $f : \mathbb{R}^2 \to \mathbb{R}^2$ *such that* $f(0) = 0$. *Let* $\lambda, \bar{\lambda}$ *be complex eigenvalues of* $Df(0)$, *such that* $|\lambda| = |\bar{\lambda}| = 1$. *If* $\lambda^k \neq 1$ *for* $k = 1, \ldots, 2l + 2$, *then there is an analytic area preserving substitution such that in the new coordinates the mapping* f *has the form* $f(r, s) = (r_1, s_1)$, *where*

$$
\begin{aligned}
r_1 &= r \cos\alpha - s \sin\alpha + O_{2l+2}, \\
s_1 &= r \sin\alpha + s \cos\alpha + O_{2l+2}, \\
\alpha &= \sum_{k=0}^{l} \gamma_k \left(r^2 + s^2\right)^k,
\end{aligned}
\tag{3}
$$

and O_{2l+2} *denotes convergent power series in* r, s *with terms of order greater than* $2l+1$, *only.*

The proof of the above theorem is constructive, i.e., given the power series for f at an elliptic fixed point one can construct explicitly an area preserving substitution and compute the coefficients $\gamma_0, \ldots, \gamma_l$ in Theorem 2.3. Explicit formulae for the third order Birkhoff normal form (case $l = 1$) will be given in Appendix A.

Now, we assume that the Algorithm 2 (`encloseNormalFormCoeffs`) realizes this procedure in the way that the following lemma holds true (and so, the Birkhoff normal form is obtained).

Lemma 2.4. *Assume that the function $P \ni p \to x_p \in [N]$ solves the implicit equation $f(p, x_p) = x_p$ in $P \times [N]$ and assume that for $p \in P$ the mapping $g(x) = f_p(x+x_p) - x_p$ satisfies the assumptions of Theorem 2.3. If Algorithm 2 is called with its arguments $(P, k, f, [N])$ and returns the interval vectors $\{[\gamma_1], \ldots, [\gamma_k]\}$, then for $p \in P$ the mapping g can be transformed by an analytic area preserving change of variables to the form Theorem 2.3 with coefficients $\hat{\gamma}_1, \ldots, \hat{\gamma}_k$ satisfying $\hat{\gamma}_i \in [\gamma_i]$ for $i = 1, \ldots, k$.*

Algorithm 2 `encloseNormalFormCoeffs`

Input:

$P \subset \mathbb{R}$: set of parameters,
$k \in \{1, 2, 3, \ldots\}$: positive integer
$f : P \times \mathbb{R}^2 \to \mathbb{R}^2$: $\mathcal{C}^1$ mapping,
$[N] \subset \mathbb{R}^2$: enclosure of the curve $p \to x_p$ solving $f(p, x_p) \equiv x_p$, for $p \in P$

Output: intervals that enclose normal form coefficients

1: computation of the Birkhoff normal form Appendix A achieving Lemma 2.4
2: **return** $\{[\gamma_1], \ldots, [\gamma_k]\}$: interval vectors

2.3. Stability of elliptic periodic orbits. An elliptic fixed point for a planar map does not need to be stable. It might happen that a strong resonance occurs, giving rise to so called Arnold diffusion and instability of the fixed point. Generically, the fixed point is stable which is the conclusion of the following classical KAM theorem.

Theorem 2.5. *[46, §32] Consider an analytic area preserving map $f : \mathbb{R}^2 \to \mathbb{R}^2$ of the form (3). If at least one of the coefficients $\gamma_1, \ldots, \gamma_l$ is not zero (*twist condition*) then the origin is a stable fixed point for f. Moreover, in any neighbourhood U containing zero there exists an invariant curve for f around the origin contained in U.*

The above beautiful result (Theorem 2.5) leads to Algorithm 3 (`verifyStability`) for validation of the existence of a branch of stable elliptic fixed points surrounded by invariant curves. It uses Algorithm 1 (`proveFixPointBranch`) for validation of the existence of a branch of fixed points and Algorithm 2 (`encloseNormalFormCoeffs`) for the computation of the Birkhoff normal form.

Lemma 2.6. *Assume the Algorithm 3 is called with its arguments $(P, k, f, [X])$ and returns* `Success`*. Then for all $p \in P$ the mapping f_p admits a unique fixed point $x_p \in [X]$. Moreover, in any neighbourhood U containing x_p there exists an invariant curve for f_p surrounding x_p and contained in U.*

Proof. If the algorithm stops and returns `Success` then the set $[N]$ (computed using `proveFixPointBranch` Algorithm 1) is nonempty and by Lemma 2.1 there exists a smooth curve of isolated fixed points $P \ni p \to x_p \in [N]$ for f_p. In line 7 of Algorithm 3 we check if the assumptions of Theorem 2.3 are fulfilled. Then, after successful computation of the Birkhoff normal form (computed using `encloseNormalFormCoeffs` (Algorithm 2)) the algorithm validates in line 11 that assumptions of Theorem 2.5 are satisfied. If so, then the assertion follows from Theorem 2.5 for all parameters $p \in P$. ∎

Algorithm 3 `verifyStability`

Input:
$P \subset \mathbb{R}$: interval of parameters,
$k \in \{1, 2, 3, \ldots\}$: positive integer
$f : P \times \mathbb{R}^2 \to \mathbb{R}^2$: $\mathcal{C}^1$ mapping,
$[X] = [a, b] \times [c, d] \subset \mathbb{R}^2$: an interval vector in which we expect the existence of a unique curve $p \to x_p$ solving $f(p, x_p) \equiv x_p$, for $p \in P$

Output: {`Success, POFailure, StabilityFailure`}

$[N] \leftarrow$ `proveFixPointBranch`$(P, f, [X])$ ▷ Algorithm 1
if $[N] = \emptyset$ **then**
  return `POFailure`
end if
$[A] \leftarrow \square D_x f(P, [N])$ ▷ interval hull of set of derivatives
$[\lambda] \leftarrow$ enclosure of the set of eigenvalues of $[A] - I$
if $[\lambda^i]$ contains 1 for some $i = 1, 2, \ldots, 2k + 2$ **then**
  return `StabilityFailure`
end if
$\{[\gamma_1], \ldots, [\gamma_k]\} \leftarrow$ `encloseNormalFormCoeffs`$(P, k, f, [N])$ ▷ Algorithm 2
if $[\gamma_i]$ does not contain zero for some $i = 1, \ldots, k$ **then**
  return `Success`
end if
return `StabilityFailure`

2.4. Resonances. In the continuation of families of periodic orbits (or fixed points of maps) several bifurcations may occur. We say a periodic orbit is resonant if there exists a constant $k \in \mathbb{N}$ such that a complex Floquet multiplier μ is such that $|\mu|^k = 1$. The smallest value of k is the *order* or *local multiplicity* of the resonance. At such values of a parameter different bifurcations may occur. In Figure 3 we present 2D phase plots of the generic standard bifurcations [2, 14, 30, 40]. We remark that some special bifurcations may appear in the case of symmetric systems [4, 21].

Among all the resonances we distinguish the case of *strong resonances* [2, 14, 30, 35] (cases with $k \in 1, 2, 3, 4$, see Figure 3). Note that when $k = 1$ or 3 a strongly resonant periodic orbit is generically unstable, whereas in cases $k = 2$ and 4 both stable and unstable situations are possible (depending on the coefficients of the resonant normal form) [30]. In our proofs we avoid the case of strong resonances, as when they are not present the bifurcation scenario is generically related with the Neimark-Sacker bifurcations [35] leading the birth of a closed invariant curve from a fixed point in discrete dynamical systems. When it happens in the Poincaré map of a limit cycle, the bifurcation generates an invariant two-dimensional torus in the corresponding ODE. That is, the resonances for $k \geq 5$ are called *weak resonances* because they do not obstruct the birth of an invariant circle. And also, this is the reason why the resonances for $k \leq 4$ are called the strong resonances. At a strong resonance the dynamics cannot be reduced to the dynamics on a bifurcating invariant circle.

A quite important consequence of the bifurcations is that in case of strong resonances it is

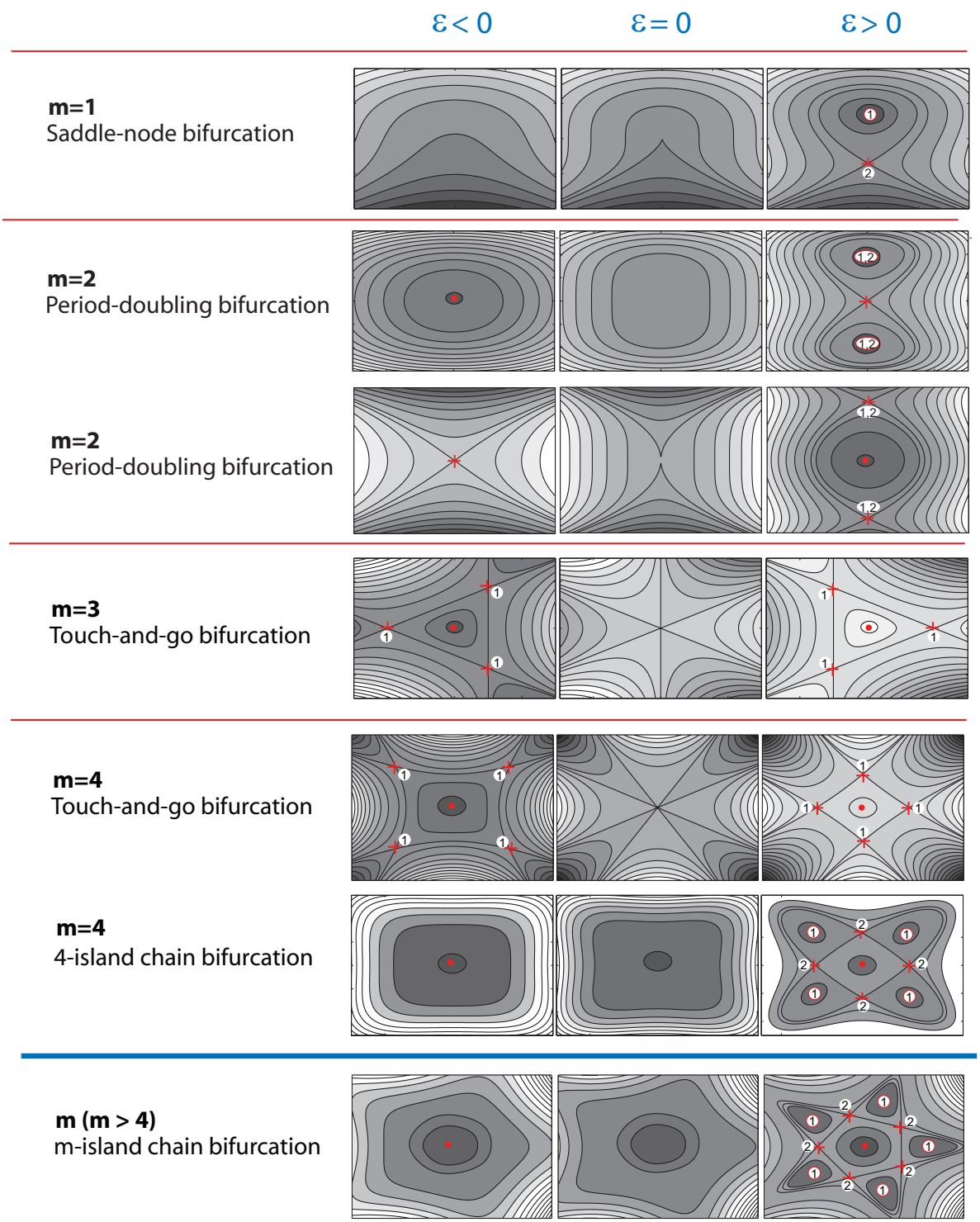

Figure 3. *Generic standard bifurcations (with respect to the parameter ε).*

not possible to provide a Computer-Assisted Proof with our algorithm, and so, some gaps will appear in the obtained CAP results. In the case of weak resonances, a resonant periodic orbit is generically (Lyapunov) stable and the chain of islands (see Figure 3) is created without touching the centre, allowing our Computer-Assisted Proof.

It is important to remark that if an elliptic fixed point of an area preserving map is near a strong resonance, the computation of the Birkhoff normal form, although theoretically possible, may be very difficult due to so called *small denominators*. The change of variables that leads to the normal form contains terms of the form $\lambda^i - 1$ in the denominator. Given that, in order to have a rigorous bound for the normal form, we must take into account all the overestimation, and so the bounds of these terms become intervals containing zero, making rigorous computation of the normal form impossible. This phenomenon is the source of gaps in the parameter range which appear in Theorem 1.1 (and in the rest of the examples).

3. Adaptive subdivision of parameter range.

In this section we discuss several improvements of Algorithm 3 in order to decrease the computational complexity, or simply to work in more cases. The Algorithm 3 has two important arguments: P and $[X]$. These arguments must be balanced: if the set $[X]$ is large, then usually it is easier to verify the existence of a family of periodic points; on the other hand, the computed bounds for the coefficients of the normal form will contain bigger overestimation and the assumptions of Theorem 2.5 may fail.

The most obvious option, naive subdivision, like a bisection, can be very inefficient. One needs an algorithm that adapts arguments P and $[X]$ of Algorithm 3 in a more continuous way. In Algorithm 4 (`processParamLeftToRight`) we provide an adaptive method that uses internally Algorithm 3 in smaller subintervals of parameters.

Note that in the Algorithm 4 we still have some undefined constants. These constants can be tuned by the user and must satisfy the following constraints

- SUCCESS_PARAM, SUCCESS_SIZE > 1
- FAILURE_PARAM, FAILURE_SIZE $\in (0, 1)$
- $h_{\min} > 0$ and $s_{\min} > 0$

In our tests, we have found the following parameter values to work well in practice:

- SUCCESS_PARAM = SUCCESS_SIZE $= 1.01$
- FAILURE_PARAM = FAILURE_SIZE $= 0.95$

Constants $s_{\min}, h_{\min}$ are used to guarantee that the algorithm always stops. They clearly depend on the user preferences and the specific problem. For instance, when one needs to verify the existence of a branch of stable fixed orbits close to some bifurcation points (like period-doubling) then these constants must be sufficiently small.

In Algorithm 4 we assume that a non-rigorous routine `findApproxFixedPoint`, which finds a good candidate for a fixed point of a map, is given. In our implementation this routine uses the continuation method together with the classical Newton method for finding zeros of multivariate maps.

Lemma 3.1. *Assume that Algorithm 4 is called with its arguments (P, f, s, h, k). Then the algorithm always stops and returns an interval $[Q]$ such that for $p \in [Q]$ the mapping f_p has stable fixed point x_p. Moreover, in any neighbourhood U containing x_p there exists an invariant curve for f_p surrounding x_p and contained in U.*

Algorithm 4 `processParamLeftToRight`

Input:
$P = [a, b] \subset \mathbb{R}$: interval of parameters,
$f : P \times \mathbb{R}^2 \to \mathbb{R}^2$: $\mathcal{C}^1$ mapping,
$s > 0$: initial size of the set,
$h > 0$: initial diameter of parameter range,
$k \in \{1, 2, 3, \ldots\}$: positive integer

Output: an interval of parameters on which the existence of stable periodic solutions was validated

$L \leftarrow a$
counter $\leftarrow 0$
repeat
  $R \leftarrow \min(a + h, b)$
  $p_0 \leftarrow \frac{1}{2}(L + R)$
  $x_0 \leftarrow$ `findApproxFixedPoint`(f_{p_0}) ▷ External nonrigorous Algorithm
  $[X] \leftarrow x_0 + [-s, s]^2$
  switch `verifyStability`$([L, R], k, f, [X])$ **do** ▷ Algorithm 3
    case `Success`
      $L \leftarrow R$
      $h \leftarrow h \cdot$ SUCCESS_PARAM
      $s \leftarrow s \cdot$ SUCCESS_SIZE
      counter $\leftarrow$ *counter* $+ 1$
    case `StabilityFailure`
      $h \leftarrow h \cdot$ FAILURE_PARAM
      $s \leftarrow s \cdot$ FAILURE_SIZE
      if $h < h_{\min}$ **then**
        $h \leftarrow h_{\min}$
      end if
    case `POFailure`
      $h \leftarrow h \cdot$ FAILURE_PARAM
until $L \geq b$ **or** $s < s_{\min}$ **or** $h < h_{\min}$
if *counter* > 0 **then**
  return $[a, L]$
end if
return $\emptyset$

Proof. First, we will show that the algorithm always stops. We observe that the number of calls to `verifyStability` (Algorithm 3) for which this algorithm returns `Success` is finite. The reason is that in the `Success` case the value L is increased by at least $h_{\min} > 0$, except when $L + h > b$, which implies $R = b$. In the last situation, the value of L is set to b and the algorithm must stop due to the condition $L \geq b$ in the loop.

Now, we assume that the algorithm does not stop. Then, there exists an iteration $i > 0$ of the main loop such that each subsequent call to `verifyStability` returns either

`StabilityFailure` or `POFailure`. In both cases the value of h is reduced by a factor FAILURE_PARAM which is assumed to be in the interval $(0, 1)$. Therefore, after a finite number of loop executions the value of h will satisfy $h \leq h_{\min}$.

In the case $h < h_{\min}$ the algorithm will stop. In the case $h = h_{\min}$ the subsequent iterations will reduce either h (then algorithm stops) or s by a factor FAILURE_SIZE which is assumed to be in the interval $(0, 1)$. Therefore, after a finite number of loop iterations either $h < h_{\min}$ or $s < s_{\min}$ will be satisfied. Thus, the algorithm must stop after a finite number of loop iterations.

So, it remains to show that the value returned by the algorithm satisfies all the required properties. Let $Q(L)$ be the following predicate: *for all parameter values* $p \in [a, L]$ *the assertion of the theorem holds true.* We will show that

$$(counter = 0 \wedge a = L) \vee (Q(L) \wedge counter > 0) \tag{4}$$

is a loop invariant. Clearly it is true before the loop because *counter* is set to zero and L is set to a. Observe that the condition $counter \geq 0$ is always satisfied since the variable *counter* is never decreased in the loop.

Variables L and *counter* are changed in the loop only in the case when the inner algorithm `verifyStability` returns `Success`. In this case, by Lemma 2.6, the assertion of theorem holds true for all parameter values $p \in [L, R]$. Assuming (4) is true before the loop iteration, we have two cases: either $counter = 0 \wedge a = L$ or $Q([a, L]) \wedge counter > 0$.

In the case $counter = 0 \wedge a = L$, to call to `verifyStability` guarantees that $Q(R)$ holds true. Therefore after setting $L = R$ and increasing *counter* we have that $Q(L) \wedge counter > 0$ is true after the loop iteration.

We consider now the second case. Assumption $Q(L) \wedge counter > 0$ implies that the assertion of theorem holds true for $p \in [a, L]$. From Lemma 2.6 it holds true for $p \in [L, R]$. Thus $Q(R)$ is satisfied. Therefore, after setting $L = R$ and increasing *counter*, we have that $Q(L) \wedge counter > 0$ holds true.

Thus, (4) is a loop invariant. After the loop finishes we have that either $counter = 0$ or $counter > 0$. In the first case the algorithm returns an empty set and thus the assertion of theorem holds true. If $counter > 0$ then due to (4) we have that $Q(L)$ holds true. Therefore for all $p \in [a, L]$ the assertion of the theorem holds true, that completes the proof. ∎

In a similar way, we can define an algorithm `processParamRightToLeft` (Reverse Algorithm 4) which scans the initial parameter $P = [a, b]$ from the right end b and returns either an empty set or an interval $[L, b]$ of parameters for which the existence of stable periodic solutions for a given map surrounded by invariant curves is validated.

4. Concurrent algorithm. In the previous section we have defined two algorithms (Algorithm 4 and Reverse Algorithm 4)

`processParamLeftToRight`
`processParamRightToLeft`

that can be used to scan a wide range of parameter values of the system and for validation of the existence of stable periodic orbits. These algorithms are sequential and they strongly use the fact that parameters of the Algorithm 3 (`verifyStability`) should not vary too much when we continue the validation over the parameter range with relative small parameter steps.

In order to speed up all the Computer-Assisted Proof process, and to use properly new computer technologies, we have to develop new adapted strategies. A concurrent version of the algorithm `verifyStability` must take into account that for some parameter ranges the verification will be very fast (time measured in seconds) while in other ranges execution time has to be measured in days (if $s_{\min}$ and $h_{\min}$ are small enough). In this section first we will propose another sequential version of the main algorithm that allows an easy parallelization (Algorithm 5), and later on we will add concurrency to it.

Algorithm 5 `processParam`

Input:

struct `ParamData` **do**
$s > 0$
$h > 0$
P : interval
$dir \in \{$`LeftRight, RightLeft`$\}$
end struct
$f : [a, b] \times \mathbb{R}^2 \to \mathbb{R}^2 : \mathcal{C}^1$ mapping,
$k \in \{1, 2, 3, \ldots\}$: positive integer,
Q : nonempty queue of objects of type `ParamData`

Output:

V: subset of $[a, b]$ on which the existence of stable periodic solutions was validated

1: $V \leftarrow \emptyset$
2: **while** Q is not empty **do**
3: $(s, h, P, dir) \leftarrow$ `dequeue`(Q)
4: **if** $dir =$ `LeftRight` **then**
5: $v \leftarrow$`processParamLeftToRight` (P, f, s, h, k) ▷ Algorithm 4
6: $newdir =$ `RightLeft`
7: **else**
8: $v \leftarrow$`processParamRightToLeft` (P, f, s, h, k) ▷ Reverse Algorithm 4
9: $newdir =$ `LeftRight`
10: **end if**
11: $V \leftarrow V \cup v$
12: $[c, d] \leftarrow \overline{P \setminus v}$
13: **if** $[c, d] \neq \emptyset$ **and** $[c, d] \neq P$ **and** $d - c \geq h_{\min}$ **then**
14: `enqueue`$(Q,$`ParamData`$(s, h, [c, d], newdir))$
15: **end if**
16: **end while**
17: **return** V

Lemma 4.1. *Assume the Algorithm 5 is called with its arguments (f, k, Q) such that for $(s, h, [c, d], dir) \in Q$ it holds that $[c, d] \subset [a, b]$ and $d - c \geq h_{\min}$. Then Algorithm 5 always stops and returns a set $V \subset [a, b]$ such that for every $p \in V$ the mapping f_p has a stable fixed point x_p. Moreover, in any neighbourhood U containing x_p there exists an invariant curve for f_p surrounding x_p and contained in U.*

Proof. The assertion on the set V follows from Lemma 3.1 because V is union of intervals returned by the two algorithms introduced in Section 3: `processParamLeftToRight` and `processParamRightToLeft` (Algorithm 4 and Reverse Algorithm 4).

We have to show that the algorithm always stops. We may assume that Q is not empty. Let W_i be the total width of the parameter intervals enqueued in Q after the i-th iteration of the main loop and let W_0 be initial width, which by our assumptions is a positive number.

By the assumptions and the construction of the algorithm it follows that each object enqueued in Q has the corresponding interval $[c, d]$ of parameters wider than $h_{\min}$. If $v = \emptyset$ then no new set is enqueued to Q. Therefore $W_i < W_{i-1} - h_{\min}$.

If $v \neq \emptyset$ then, by the construction of Algorithm 4 (`processParamLeftToRight`) and Reverse Algorithm 4 (`processParamRightToLeft`), we have that the width of the interval v is greater than $h_{\min}$. Thus, even if we enqueue a new interval $[c, d]$ to Q, we have that $W_i < W_{i-1} - h_{\min}$. Therefore, after a finite number of iterations we must have $W_i < h_{\min}$. Given that each set in Q has the corresponding interval $[c, d]$ of parameters wider than $h_{\min}$, this is possible only if Q is empty. Then the loop is finished. ∎

Observe that when we enqueue a new element to Q in Algorithm 5 then the parameters h, s are the same as for the initial interval of parameters. This is reasonable since we were not able to validate the entire interval P and probably there is a bifurcation in it. Therefore, processing of the remaining part of this interval from the second endpoint is an independent task.

Algorithm 5 can be easily parallelized by applying the *producer-consumer* model. Nevertheless, straightforward implementation by using of concurrent queue and many threads requesting new data to process might be very inefficient.

It might happen (and usually does) that Q is empty and all the threads but one are idle, and the only running thread is processing its interval for a very long time. We can solve this problem by slight modifications of the algorithms `processParamLeftToRight` and `processParamRightToLeft`. Namely, in the case when the call to `verifyStability` returns `Success` we can additionally check whether there is an idle task waiting for data to process. In this case, a thread can split the remaining (unchecked yet) parameter range and enqueue it for execution in other waiting thread. We would like to emphasise here that at this point we must use information on current parameters s and h. Otherwise, balancing them can take some nontrivial time and the profits from parallelization might be artificial. In fact, we observed that execution time of the program running on 8 CPUs was almost the same as of sequential version when we did not take into account continuation of parameters s and h.

The current implementation of the algorithm contains more sophisticated improvements that are too technical to be presented here and they are out of the scope of this article. We will mention only that we needed to manage gaps in the parameter range, use adaptation of the parameter k (order of the Birkhoff normal form) and many others.

5. First example: proof of Theorem 1.1 on the existence of a invariant tori for the forced pendulum system. A first example of applicability of the algorithms was shown in the introduction with a theorem (Theorem 1.1) presenting a Computer-Assisted Proof of the existence and stability of elliptic periodic orbits and invariant tori for a periodically forced pendulum (that is, a 2D non-autonomous Hamiltonian). In this section we give the proof of

Theorem 1.1:

Proof. [**Theorem 1.1**] Let us denote by $P_\omega : \mathbb{R}^2 \multimap \mathbb{R}^2$ a family of maps given by $P_\omega(\theta, \dot{\theta}) = \varphi(2\pi/\omega, \theta, \dot{\theta})$, where $\varphi : \mathbb{R} \times \mathbb{R}^2 \multimap \mathbb{R}^2$ is a local flow induced by (2). We will call P_ω the Poincaré map. Let us observe, that (2) is a non-autonomous Hamiltonian system. Therefore, P_ω is an area preserving map, wherever it is well defined.

We ran Algorithm 5 with the parameter values $s_{\min} = h_{\min} = 10^{-14}$ and with the parameter range $P = \Omega \equiv [1, 31]$ as defined in (1).

Table 1

Results from Algorithm 5 applied to the Poincaré map for the periodically forced pendulum (2). Column $\#\Omega$ contains the number of subintervals used in the CAP in the corresponding parameter range. The third column gives the coefficients of the normal form.

parameter intervals	$\#\Omega$	normal form coefficients
$\Omega_7 \equiv 0.^{31000000000000000000}_{03997772676398706266} \cdot 10^2$	27142	$\gamma_1 \subset [0.0252729, 0.196686]$
$G_4 \equiv 0.39977726763982^{706266}_{326566} \cdot 10^1$	–	(1:4 resonance)
$\Omega_6 \equiv 0.^{3997772676398326566}_{2996123279252236766} \cdot 10^1$	1391	$\gamma_1 \subset [6.44355\texttt{e-}05, 0.326523]$
$\Omega_5 \equiv 0.2996^{123279252236766}_{032828150809299} \cdot 10^1$	32	$\gamma_1 \subset [-0.0233358, 0.0210311]$ $\gamma_2 \subset [16.5368, 86.3966]$
$\Omega_4 \equiv 0.299^{60328281508092 99}_{4091684028588500} \cdot 10^1$	1364	$\gamma_1 \subset [-1.82011\texttt{e+}08, -1.21537\texttt{e-}05]$
$G_3 \equiv 0.2994091684^{28588500}_{12414777} \cdot 10^1$	–	(1:3 resonance)
$\Omega_3 \equiv 0.^{2994091684012414777}_{1970242591584483455} \cdot 10^1$	2211444	$\gamma_1 \subset [0.000714712, 1.84162\texttt{e+}08]$
$G_2 \equiv 0.19702425^{91584483455}_{101046491000} \cdot 10^1$	–	(1:2 resonance—period-doubling)
$\Omega_2 \equiv 0.1^{970242101046491000}_{018227823641081788} \cdot 10^1$	8245005	$\gamma_1 \subset [-5.85576, -3.7844\texttt{e-}08]$
$G_1 \equiv 0.10182275^{823641081788}_{398927290977} \cdot 10^1$	–	(1:2 resonance—period-doubling)
$\Omega_1 \equiv 0.10^{18227398927290977}_{00000000000000000} \cdot 10^1$	6807817	$\gamma_1 \subset [1.18609\texttt{e-}06, 2.05016]$

In Table 1 we show the coefficients obtained with the algorithm. The first column denotes the different parameter intervals Ω_i where the Algorithm 5 has been able to obtain a positive answer (that is, `verifyStability` returns `Success`). The union of all these subintervals gives us $\overline{\Omega \setminus (G_1 \cup G_2 \cup G_3 \cup G_4)}$, where G_1, G_2, G_3 and G_4 are the four gaps in the entire parameter range $\Omega = [1, 31]$ we examined. In these gaps, different *strong resonances* appear (see Subsection 2.4), and it is the situation where the Algorithm 2 (`encloseNormalFormCoeffs`) does not work. The second column denotes the cardinal $\#\Omega$, that is, the number of subintervals used in the CAP in the corresponding parameter range. Note that it is proved that the coefficient γ_1 in the normal form (third column) is not vanishing for all but one subintervals (Ω_5), where we had to check also the condition $\gamma_2 \neq 0$. Therefore, Theorem 2.5 can be applied, and thus, we obtain a Computer-Assisted Proof of Theorem 1.1 about the existence and stability of

elliptic periodic orbits and invariant tori. ■

6. Application to reversible systems: the Michelson system. The existence of an invariant curve for a planar map $f : \mathbb{R}^2 \to \mathbb{R}^2$ can be proved without assuming that f is measure preserving. The key assumption in the proof given in [46] is that any curve γ around an elliptic fixed point intersects its image under f, i.e. $f(\gamma) \cap \gamma \neq \emptyset$. This condition is satisfied for reversible planar maps around a symmetric elliptic fixed point.

Before giving the proof of the main result of this section, Theorem 6.7, we recall some basic properties of reversible systems.

Definition 6.1. *An invertible transformation $S : \Omega \longrightarrow \Omega$ is called a* reversing symmetry *of a local dynamical system $\phi : \mathbb{T} \times \Omega \longrightarrow \Omega$, $\mathbb{T} = \mathbb{R}$ or $\mathbb{T} = \mathbb{Z}$, if the following conditions are satisfied:*

1. *if $(t, x) \in \mathrm{dom}\,(\phi)$ then $(-t, S(x)) \in \mathrm{dom}\,(\phi)$,*
2. *$S(\phi(t, x)) = \phi(-t, S(x)))$.*

Remark 6.2. *In the discrete time case, the above two conditions are equivalent to the following identity*

$$S \circ f = f^{-1} \circ S.$$

where $f = \phi(1, \cdot)$ is a generator of ϕ.

Definition 6.3. *Let $\phi : \mathbb{T} \times \Omega \to \Omega$ be a local (discrete or continuous) dynamical system. For $x \in \Omega$ we define the sets*

$$I(x) = \{t \in \mathbb{T} : (t, x) \in \mathrm{dom}\,(\phi)\},$$
$$\mathcal{O}(x) = \{\phi(t, x) \in \Omega : t \in I(x)\}.$$

The set $\mathcal{O}(x)$ will be called the orbit *of x.*

Definition 6.4. *Assume S is a reversing symmetry for $\phi : \mathbb{T} \times \Omega \to \Omega$. An orbit $\mathcal{O}(x)$ is called* S-symmetric *if $\mathcal{O}(x) = S(\mathcal{O}(x))$.*

Remark 6.5. *[36] In the continuous case, the orbit $\mathcal{O}(x)$ is S-symmetric if it contains a point from the set* $\mathrm{Fix}(S) = \{y : S(y) = y\}$.

Remark 6.6. *[53, Lemma 3.3] It is easy to see that if $\Theta \subset \Omega$ is a Poincaré section for an R-reversible flow $\phi : \mathbb{R} \times \Omega \to \Omega$ such that $\Theta = R(\Theta)$, then the Poincaré map $P : \Theta \to \Theta$ is $R|_\Theta$-reversible.*

A well known method for proving the existence of an R-symmetric periodic solution in an R-reversible system is the shooting method, also called *fixed set iteration method* [36, 55]. Assume f is an R-reversible map, where R is an involution, i.e. $R = R^{-1}$. Then $(f \circ R)^2(x) = x$, wherever the left side is well defined. Let x be such that

$$x \in \mathrm{Fix}(R), \quad f(x) \in \mathrm{Fix}(R).$$

Then

$$x = \mathrm{Id}(x) = (f \circ R)^2(x) = f^2(x)$$

holds and x is a periodic point for f. Since $x \in \mathrm{Fix}(R)$ the orbit of x is R-symmetric.

We will use this simple previous idea to prove the existence of symmetric periodic solutions for the Michelson system [41] given by $x''' + x' + \frac{1}{2}x^2 = c^2$ or by the equivalent first ODE system

$$\left\{ \begin{array}{rcl} \dot{x} &=& y, \\ \dot{y} &=& z, \\ \dot{z} &=& c^2 - y - \frac{1}{2}x^2. \end{array} \right. \tag{5}$$

This system is an equation for the steady state solution of the one-dimensional Kuramoto-Sivashinsky PDE. On the other hand, this system appears also as a part of the limit family of the unfolding of the nilpotent singularity of codimension three (see [25]).

The system (5) is reversible with respect to the symmetry

$$R : (x, y, z, t) \to (-x, y, -z, -t)$$

and since its divergence vanishes, it is also volume preserving.

The dynamical system induced by (5) exhibits rich and different types of dynamics when the parameter c varies. For sufficiently large c there is a simple invariant set consisting two equilibria $(\pm c\sqrt{2}, 0, 0)$ and an heteroclinic orbit between them [39]. Lau [38] observed numerically that when the parameter c decreases a cascade of cocoon bifurcations occurs and at the limit value $c \approx 1.266232337$ a periodic orbit is born through a saddle-node bifurcation. The Computer-Assisted Proof of the existence of the cocooning cascade of heteroclinic tangencies is given in [34] and the CAP required computations of second order derivatives of a certain Poincaré map.

For the parameter value c equal to one, and slightly smaller than one, it was proved in [26, 52, 53, 54] that the system has rich dynamics including symbolic dynamics, heteroclinic solutions, Bykov cycles and Shilnikov homoclinic solutions.

The bifurcation diagram of periodic solutions presented by Michelson suggests [41, Fig.1] that for all parameter values $c \in (0, 0.3194)$ there are at least two elliptic periodic orbits. In this section we present a proof that for some range of parameter values indeed there exist elliptic periodic solutions surrounded by invariant curves. Before, we give the details let us comment about the observed dynamics of this system.

For $c = 0$ the origin is an equilibrium point of (5) with eigenvalues equal to 0 and $\pm\imath$ (being $\imath$ the imaginary unit). The dynamics of the system for $c \approx 0$ has been studied in [37]. The authors proved that an elliptic periodic orbit and an heteroclinic cycle born simultaneously giving rise to a very rich dynamics. In particular [37, Thm. 1.4] in each interval of parameters $[0, \delta)$ there is a countable infinity of homoclinic and heteroclinic solutions, periodic orbits accumulating to heteroclinic and homoclinic cycles as well as countable infinity of hyperbolic horseshoes.

For parameter values c slightly above zero there is an elliptic periodic orbit with eigenvalues of the derivative of a certain Poincaré map $\lambda_c, \overline{\lambda_c}$ such that $\lambda_c \to 1$ when $c \to 0$. When the parameter increases these eigenvalues follow the unit circle crossing two strong resonances 1:4 and 1:3 – see Figure 5. In the computer assisted approach we excluded some ranges of parameters around strong resonances - these are the two gaps G_1 and G_2 between C_1 and C_2, and, C_4 and C_5, respectively.

Apparently, for some $c_0 \approx 0.22544$ there is a bifurcation according to a 1:4 resonance and a chain of four periodic islands (see Subsection 2.4) are born as it is shown in Figure 4 - see also the movie `mpp.mov` available at [51] (and in the supplementary material) that presents an animation of the phase portrait of a Poincaré map for the parameter values from the range $[0.1, 0.25]$.

Eventually, the eigenvalues reach the second parabolic case -1 and then the periodic solution become hyperbolic.

Let us define the Poincaré section $\Pi := \{(0, z, y) : z, y \in \mathbb{R}\}$. Let $P_c = (P_1, P_2) : \Pi \multimap \Pi$ be the Poincaré map for the system with the parameter value c. Notice that P_c is in fact a half Poincaré map (in order to take profit of the symmetry), which means that the trajectory of x crosses Π in the opposite direction when passing through x and $P_c(x)$, and therefore periodic orbits for the Michelson system correspond to periodic points for P_c^2.

Since the section Π is invariant under the symmetry $(x, y, z) \to (-x, y, -z)$, from Remark 6.6 the Poincaré map is also reversible with respect to an involution $R(y, z) = (y, -z)$. We will use the same letter R to denote the reversing symmetry of the Poincaré map P_c and of the Michelson system.

Now we can state the theorem.

Theorem 6.7. *For all parameter values $c \in C$ with*

$$C \equiv [2.8927215267474 \cdot 10^{-6}, 0.3193764547298809797],$$

there exists a symmetric elliptic periodic orbit p_c for the Michelson system

$$x''' + x' + \frac{1}{2}x^2 = c^2. \tag{6}$$

Moreover, for

$$c \in C_e = \overline{C \setminus (G_1 \cup G_2)}, \tag{7}$$

where

$$G_2 \equiv 0.276343^{3967893742525}_{0638300670202} \quad \textit{(1:3 resonance)}$$
$$G_1 \equiv 0.2254404^{857280028282}_{795432195858} \quad \textit{(1:4 resonance)}$$

these orbits p_c are stable. Moreover, each neighbourhood of p_c in the full phase space (x, x', x'') contains a 2D torus surrounding p_c, separating the phase space and invariant under the flow generated by (6).

Proof. As we observed at the beginning of this section, an R-reversible planar map may have invariant curves around an R-symmetric elliptic fixed point. In the reversible case, a planar map admits the same normal form at symmetric elliptic fixed points as in the area-preserving case, and the substitution which brings the map to the normal form is exactly the same as we described in the Appendix – for details see [45, 15].

On Figure 5 a non-rigorous plot of the coefficient γ_1 of the normal form Theorem 2.3 versus the parameter c is presented. Observe that for a parameter value $c_* \approx 0.25961$ the

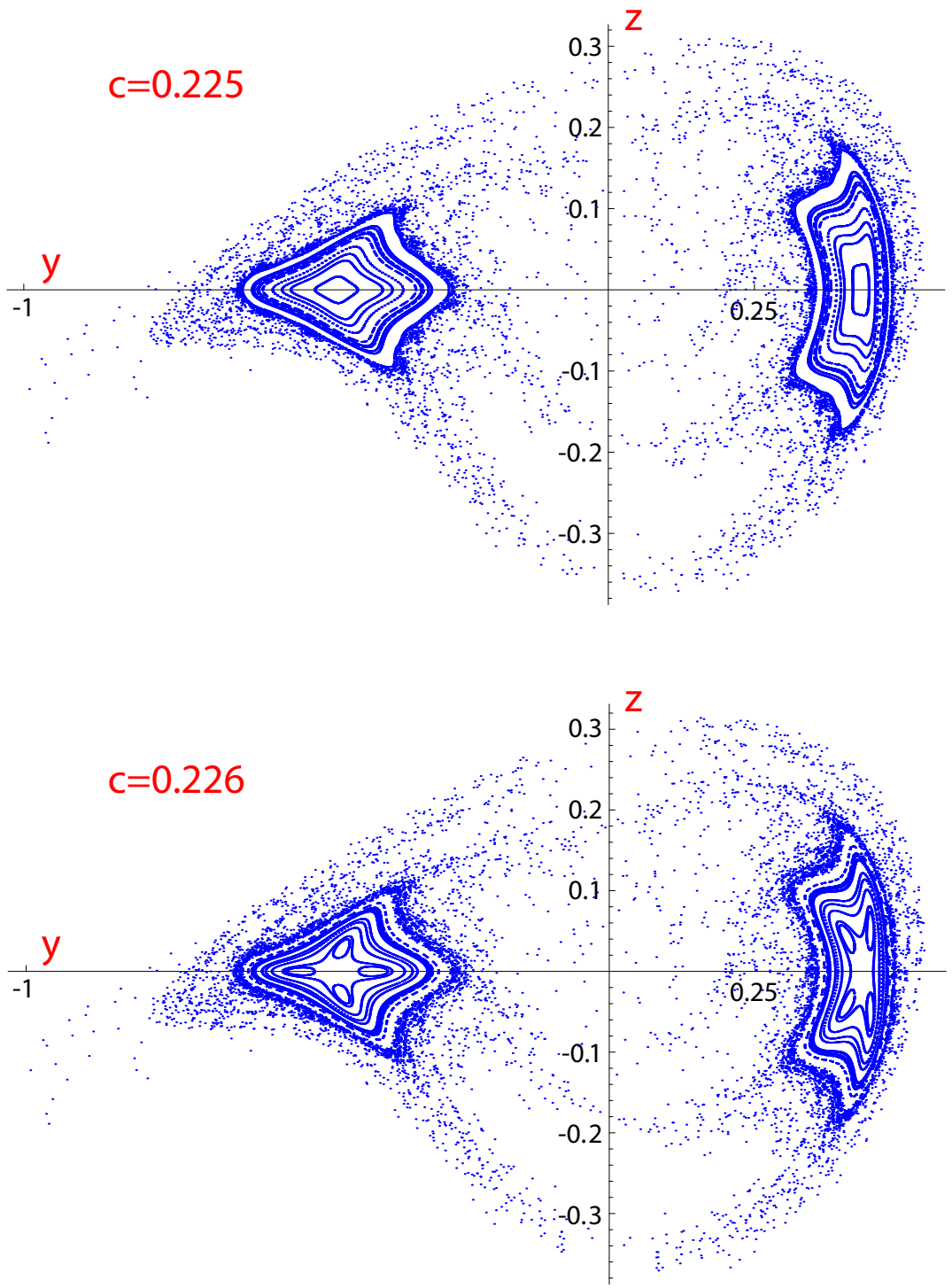

Figure 4. *Phase portrait of the half Poincaré map P_c (top) before the bifurcation for $c = 0.225$ and (bottom) after the bifurcation for $c = 0.226$ with four periodic islands. Between these parameters a strong resonance 1:4 occurs with eigenvalues equal to $\pm\imath$. See also the auxiliary material* `mpp.mov` *available at [51] (and in the supplementary material) with the animation of this phase portrait.*

Table 2

Results from Algorithm 5 applied to the Poincaré map for the Michelson system (5). Column #C contains the number of subintervals used in the CAP in the corresponding parameter range. The third column gives the coefficients of the normal form.

parameter intervals	$\#C$	normal form coefficients
$C_5 \equiv 0.^{3193764547298809797}_{2763433967893742525}$	333729	$\gamma_1 \subset [0.000970321, 1.09549\texttt{e+07}]$
$G_2 \equiv 0.276343^{3967893742525}_{0638300670202}$	–	(1:3 resonance)
$C_4 \equiv 0.2^{7634306383006702 02}_{5964385369624238 38}$	53822	$\gamma_1 \subset [-1.07988\texttt{e+07}, -1.74636\texttt{e-07}]$
$C_3 \equiv 0.259^{6438536962423838}_{5644845299308181}$	1700	$\gamma_1 \subset [-0.444065, 0.438639]$ $\gamma_2 \subset [3331.57, 11855.4]$
$C_2 \equiv 0.2^{5956448452993081 81}_{2544048572800282 82}$	29868	$\gamma_1 \subset [1.45172\texttt{e-07}, 32.4201]$
$G_1 \equiv 0.2254404^{8572800282 82}_{7954321958 58}$	–	(1:4 resonance)
$C_1 \equiv 0.^{2254047954321958 58}_{0000028927215267474}$	29807889	$\gamma_1 \subset [9.63725\texttt{e-06}, 2.33115\texttt{e+06}]$

coefficient γ_1 vanishes. Therefore, around this parameter value we need to compute the next coefficient γ_2 (this is the reason to create the interval C_3 in the proof) to satisfy the twist condition.

Application of Algorithm 5 with its accuracy parameters $h_{\min} = s_{\min} = 10^{-14}$ to the Poincaré map P_c of the Michelson system with initial parameter range $C = [0.0, 0.3194]$ gives the results listed in Table 2. The first column denotes the different parameter intervals C_i where the Algorithm 5 has been able to obtain a positive answer (that is, `verifyStability` returns `Success`). The union of all these subintervals gives us $\overline{C \setminus (G_1 \cup G_2)}$, where G_1 and G_2 are two gaps between C_1 and C_2, and, C_4 and C_5, due to the presence of *strong resonances*, in particular 1:4 and 1:3 resonances, respectively (see Subsection 2.4), and its is the situation where the algorithms do not work. The second column denotes the cardinal $\#C$, that is, the number of subintervals used in the CAP in the corresponding parameter range. Note that it is proved that the coefficient in the normal form $\gamma_1 \neq 0$ (third column), but in one subinterval (C_3) where we had to compute also $\gamma_2 \neq 0$ (see Figure 5 for a plot of the values of de coefficient γ_1). Therefore, the Theorem 2.5 works, and thus, we obtained a Computer-Assisted Proof of Theorem 6.7 about the existence and stability of elliptic periodic orbits and invariant tori. ■

The two gaps, G_1 and G_2, of Theorem 6.7 contain parameter values for which strong resonances 1:4 and 1:3 occur, respectively. In generic case these resonances occur for isolated parameter values. Since the exact value of the resonant parameter value usually cannot be computed, in a Computer-Assisted Proof we must exclude some range around the resonances. The two gaps, G_1 and G_2, as well as the right end of interval C, are returned by our algorithm. Note (see Figure 5) that for a parameter value $c \approx 0.22544$ corresponding to a 1:4 resonance a removable singularity occurs, in contrary as what happens for the 1:3 resonance at $c \approx 0.27634$, where the singularity is non-removable. This suggests that invariant curves may persist for

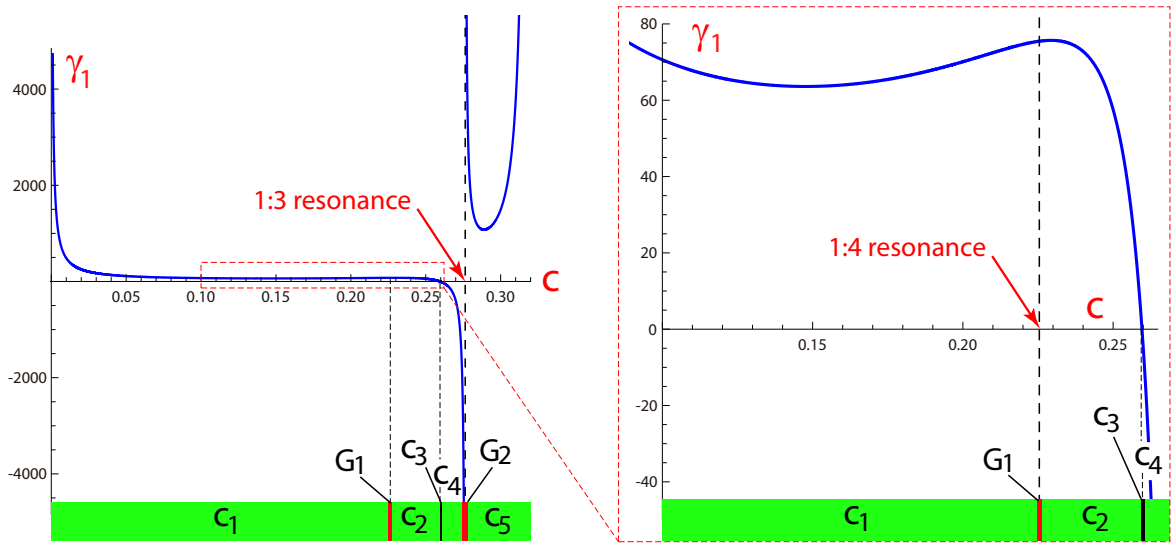

Figure 5. *Non-rigorous plot of the coefficient γ_1 in the normal form Theorem 2.3 for P_c versus the parameter. Observe, that for a parameter value $c \approx 0.22544$ corresponding to 1:4 resonance, a removable singularity occurs. This suggests that invariant curves persist for this resonant parameter value.*

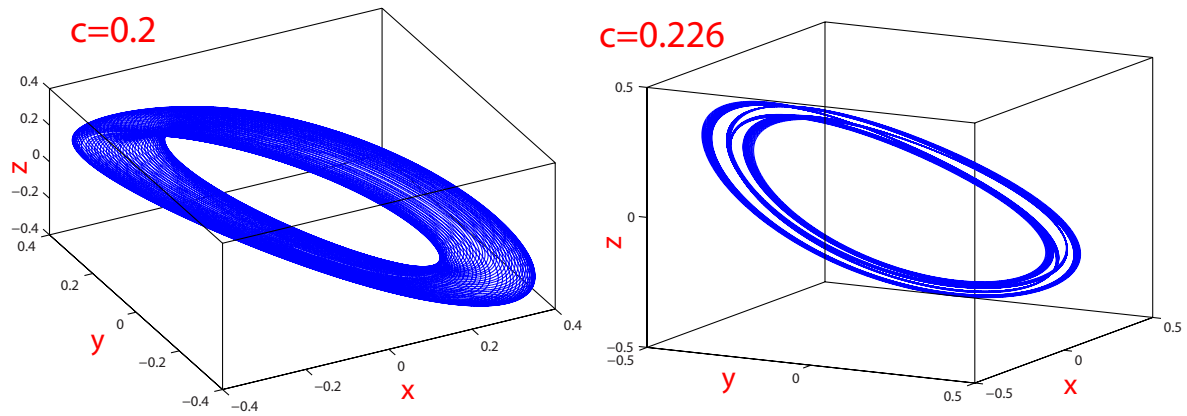

Figure 6. *Numerically observed quasi-periodic trajectory for the Michelson system (6) with $c = 0.2$ and $c = 0.226$. See also Figure 4.*

this resonant parameter value (in this case the main periodic orbit does not change its stability character as a chain of islands is created, see Figure 3 and Figure 4).

On Figure 6 two typical trajectories of the system (6) are presented. The initial conditions are taken at a neighbourhood of the existing elliptic periodic solution, giving rise to an invariant torus.

7. Application to Hamiltonian systems: the Hénon-Heiles Hamiltonian. The Hénon-Heiles (HH) system [31] represents a paradigmatic model for time-independent Hamiltonian systems with two degrees of freedom. This system defines the motion of a particle with unit mass (a star) around a galactic centre where the motion is restricted to a plane under the two dimensional potential $V(x,y) = \frac{1}{2}(x^2+y^2) + x^2y - \frac{1}{3}y^3$. Two main types of motion exist for different values of the energy: bounded and unbounded motion, and both of them can present regular or chaotic behaviour. There is a threshold value of the energy $\mathcal{H}$, called *escape energy*, $\mathcal{H}_{\text{esc}} = 1/6$, for which the particle might escape from the potential well for values of energy above it. The system presents (among others) a triangular symmetry D_3 with three different exits for which the particle may escape [5, 6].

In Figure 7 we show the skeleton of symmetric periodic orbits (imposing the initial conditions $x(0) = p_y(0) = 0$), allowing y to change, for the Hénon-Heiles problem versus the Hamiltonian (energy) constant $\mathcal{H}$ up to global multiplicity $m = 12$ (see on the legend the colour code). Note that once fixed y and $\mathcal{H}$ the initial value $p_x(0)$ is obtained from the Hamiltonian equation. The forbidden region (region where the initial conditions are not possible) is the grey area. The *skeleton* of symmetric periodic orbits has been obtained by using the grid search method taking advantage of the symmetries of the problem (for details see [4], and references [5, 6, 7] for numerical studies of the HH problem). On the plot we have remarked the strong resonances that in the next Theorem 7.1 will generate gaps, as well as the proved families of periodic orbits.

Theorem 7.1. *Consider the Hénon-Heiles hamiltonian*

$$\mathcal{H}(x,y,p_x,p_y) = \frac{1}{2}(p_x^2+p_y^2) + \frac{1}{2}(x^2+y^2) + y(x^2 - \frac{1}{3}y^2). \tag{8}$$

There exists a continuous family of stable elliptic periodic orbits for the Hénon-Heiles system parameterized by the values of Hamiltonian $\mathcal{H} \in \mathcal{H}_0$, where

$$\mathcal{H}_0 \equiv [1.69651338377777 \cdot 10^{-5}, 1/6] \setminus \operatorname{int} \bigcup_{i=1}^{5} G_i$$

and the gaps G_i are tiny open intervals enclosing apparent bifurcations and resonances

period-2 branch

$$G_5 \equiv 0.158716635^{4766920707}_{3717410202} \quad \textit{(1:3 resonance)}$$
$$G_4 \equiv 0.1545526236^{462015656}_{39517070} \quad \textit{(1:4 resonance)}$$

period-1 branch

$$G_3 \equiv 0.14865042^{76067615353}_{34126736565} \quad \textit{(1:2 resonance—period-doubling)}$$
$$G_2 \equiv 0.12721790^{18497908282}_{7454098787} \quad \textit{(1:3 resonance)}$$
$$G_1 \equiv 0.1024287842^{846403131}_{21283232} \quad \textit{(1:4 resonance)}$$

Moreover, each neighbourhood of any periodic orbit p_e in the fixed-energy submanifold $\mathcal{H}_e$ contains 2D invariant tori under the flow surrounding p_e.

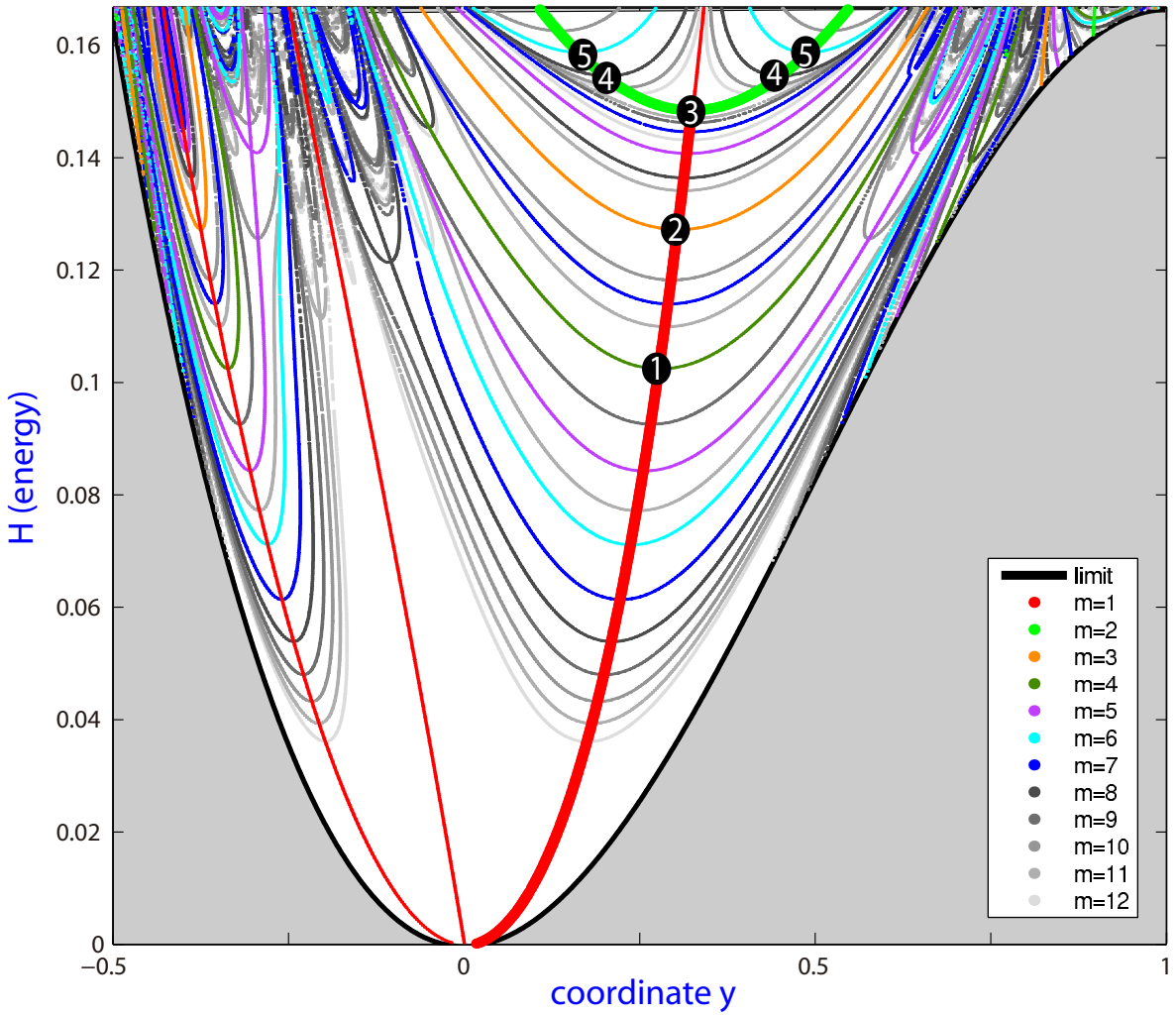

Figure 7. *Non-rigorous biparametric plot of the skeleton of symmetric periodic orbits for the Hénon-Heiles Hamiltonian. The families of periodic orbits proved in Theorem 7.1 are highlight, as the strong resonances leading gaps.*

Proof. We ran Algorithm 5 with the parameter values $s_{\min} = h_{\min} = 10^{-14}$ and with the energy range $\mathcal{H} \equiv [10^{-5}, 1/6]$. Returned results are given in Table 3. For all energy levels $\mathcal{H} \in \mathcal{H}_0$ the first normal form coefficient γ_1 exists and it is non-vanishing. Therefore, by Theorem 2.3 and Theorem 2.5 the assertion holds true.

We remark that we follow the stable branch, and thus, we begin with the period-1 branch (thick red line in Figure 7), and after the first period-doubling bifurcation (gap G_3), this bifurcation makes unstable the main orbit (see Figure 3), therefore we follow now the stable period-2 branch (thick green line in Figure 7).

In papers [10, 9] we provided rigorous proofs and methodology of the existence of complete

Table 3

Results from Algorithm 5 applied to the Poincaré map for the Hénon-Heiles system (8). Column #H contains the number of subintervals used in the CAP in the corresponding parameter range. The third column gives the coefficients of the normal form.

parameter intervals	$\#H$	normal form coefficients
$H_6 \equiv 0.1^{6666666666666969}_{5871663547669207 07}$	30650	$\gamma_1 \subset [0.00134049, 1157.47]$
$G_5 \equiv 0.15871663 5^{4766920707}_{3717410202}$	–	(1:3 resonance)
$H_5 \equiv 0.15^{87166353717410202}_{45526236462015656}$	22318	$\gamma_1 \subset [0.00189182, 2163.23]$
$G_4 \equiv 0.154552623 64^{62015656}_{39517070}$	–	(1:4 resonance)
$H_4 \equiv 0.1^{545526236439517070}_{486504276067615353}$	254736	$\gamma_1 \subset [0.0618411, 3.052\texttt{e+09}]$
$G_3 \equiv 0.1486504 2^{76067615353}_{34126736565}$	–	(1:2 resonance—period-doubling)
$H_3 \equiv 0.1^{4865042341267365 65}_{2721790184979082 82}$	46685	$\gamma_1 \subset [0.0314925, 6.29043\texttt{e+13}]$
$G_2 \equiv 0.12721790 1^{8497908282}_{7454098787}$	–	(1:3 resonance)
$H_2 \equiv 0.1^{272179017454098787}_{024287842846403131}$	43750	$\gamma_1 \subset [0.0400474, 96.2272]$
$G_1 \equiv 0.1024287842 8^{46403131}_{21283232}$	–	(1:4 resonance)
$H_1 \equiv 0.^{1024287842821283232}_{0000169651338377777}$	11209094	$\gamma_1 \subset [2.44444\texttt{e-07}, 87.7133]$

skeletons of periodic orbits for the Hénon-Heiles system. The Theorem 7.1 goes farther as it provides a proof of families of periodic orbits in the skeleton of periodic orbits shown in Figure 7, but it also provides a proof of the existence of surrounding tori and the stability of the orbits (the existence of the invariant tori was not obtained before around a family of periodic orbits).

8. Accuracy versus time of computation. In the previous sections we have shown the applicability of our method to three ODEs of different types. In each case, the actual intervals of parameters and gaps were returned by the routine. In this section we will discuss the impact of the two parameters $h_{\min} > 0$ and $s_{\min} > 0$ of the Algorithm 4 onto the final result and the time of computation.

These parameters stand for the smallest allowed parameter range examined at once and the smallest acceptable set for the interval Newton operator in validation of the existence of a periodic orbit. Clearly, smaller values of these parameters give a chance to compute enclosures to the coefficient in the normal γ_1 with higher accuracy and, in consequence, allow to enlarge the set of parameters for which the existence of a stable periodic orbit surrounded by invariant tori is validated.

In Table 4, Table 5 and Table 6 we present the results of our numerical test. For each one of the three ODEs we have considered in previous sections, we run Algorithm 5 with various values of $h_{\min}$ and $s_{\min}$. For fixed values of $h_{\min}$ and $s_{\min}$ we list the total time of

Table 4

Time of computation and the total measure of parameters for which Algorithm 5 applied to the Poincaré map of the forced pendulum equation (2) returned `Success`*. First column are the parameters $h_{min} = s_{min}$ of the algorithm.*

Forced pendulum equation (2)			
$h_{\min} = s_{\min}$	wall time (minutes)	total measure	relative measure
10^{-4}	0.99	29.6730233974213	$\approx 98.91007799\%$
10^{-5}	1.89	29.8322603946307	$\approx 99.44086798\%$
10^{-6}	6.04	29.9951865874871	$\approx 99.98395529\%$
10^{-7}	7.25	29.9989523246606	$\approx 99.99650775\%$
10^{-8}	9.47	29.9996790103979	$\approx 99.99893003\%$
10^{-9}	13.14	29.9999018872286	$\approx 99.99967296\%$
10^{-10}	20.65	29.9999684027933	$\approx 99.99989468\%$
10^{-11}	38.63	29.9999899376452	$\approx 99.99996646\%$
10^{-12}	88.69	29.9999966501278	$\approx 99.99998883\%$
10^{-13}	223.2	29.9999986713898	$\approx 99.99999557\%$
10^{-14}	784.6	29.9999990847316	$\approx 99.99999695\%$

computation and the total measure of the set of parameters for which the stability has been verified. We observe, that in each case more than 99.9% of the final measure of the parameter space can be obtained within reasonable short time of computation - here less than 80 minutes. Decreasing parameters $h_{\min}$ and $s_{\min}$ of the algorithm allows us to get closer and closer to the detected bifurcations or resonances making the gaps around them much thinner. This does not, however, increase significantly the total measure of the parameter range as it is already quite close to the 100%, but we can observe that with enough precision and CPU time the total measure approaches to the whole one.

All the computations were performed on a computer equipped with 120 processors Intel(R) Xeon(R) CPU E7-8867 and 512GB of memory and the time of computation given in Table 4, Table 5 and Table 6 is the actual running time on this machine.

9. Conclusions. In this paper we have shown that the rigorous computation of higher order derivatives of return maps is a powerful tool in the study of dynamics around elliptic periodic solutions. We have presented, for area preserving planar maps, an algorithm and a complete methodology for rigorous validation of the existence of continuous branches of stable elliptic fixed points and the existence of invariant tori surrounding them.

With the help of the algorithm we have given new rigorous results about the existence of continuous branches of stable periodic orbits and invariant tori surrounding them for three

Table 5

Time of computation and the total measure of parameters for which Algorithm 5 applied to the Poincaré map of the Michelson system (5) returned `Success`*. First column are the parameters $h_{min} = s_{min}$ of the algorithm.*

Michelson system (5)			
$h_{\min} = s_{\min}$	wall time (minutes)	total measure	relative measure
10^{-6}	0.79	0.285999130019116	$\approx 89.54822782\%$
10^{-7}	1.55	0.314805502453802	$\approx 98.56769442\%$
10^{-8}	3.09	0.318555147945601	$\approx 99.74173334\%$
10^{-9}	4.74	0.319156513375934	$\approx 99.93002485\%$
10^{-10}	8.61	0.319310315650539	$\approx 99.97818137\%$
10^{-11}	18.30	0.319354868547584	$\approx 99.99213118\%$
10^{-12}	47.23	0.319368400906037	$\approx 99.99636825\%$
10^{-13}	132.8	0.319372705635205	$\approx 99.99771609\%$
10^{-14}	223.2	0.319373222864263	$\approx 99.99787803\%$

Table 6

Time of computation and the total measure of parameters for which Algorithm 5 applied to the Poincaré map of the Hénon-Heiles system (8) returned `Success`*. First column are the parameters $h_{min} = s_{min}$ of the algorithm.*

Hénon-Heiles system (8)			
$h_{\min} = s_{\min}$	wall time (minutes)	total measure	relative measure
10^{-6}	38.46	0.107869349671606	$\approx 64.721609803\%$
10^{-7}	59.61	0.163912987511601	$\approx 98.347792507\%$
10^{-8}	80.75	0.165867464513602	$\approx 99.5204787082\%$
10^{-9}	112.7	0.166382976854234	$\approx 99.8297861125\%$
10^{-10}	182.9	0.166558337452625	$\approx 99.9350024716\%$
10^{-11}	359.5	0.166623869854324	$\approx 99.9743219126\%$
10^{-12}	912.3	0.166649668677243	$\approx 99.9898012063\%$
10^{-13}	947.7	0.166649693342073	$\approx 99.9898160052\%$
10^{-14}	1084	0.166649697124647	$\approx 99.9898182748\%$

classical problems: the periodically forced pendulum equations, the Michelson system and the Hénon-Heiles Hamiltonian.

However, many questions remain open that are part of our near future research. One interesting task is to describe the dynamics of the map for the resonant parameter values. For example, the presence of a strong resonance 1:4 may lead either to instability of an elliptic fixed point or the invariant tori may persist. This depends on the actual coefficients in so called resonant normal form [24, 47]. Another interesting problem is the estimation of the size (in some appropriate sense) of quasi-periodic islands around an elliptic periodic point. The KAM theory gives only a local information; in a sufficiently small neighbourhood of an elliptic periodic point invariant curves exist, provided normal form satisfies the twist condition. We believe that the computation of the normal form, together with the rigorous estimation of the radius of convergence of the change of coordinates, may give a positive answer to this problem.

Appendix A. Explicit formula for the coefficients in third order normal form. Below we show an explicit formula (for details see the classical reference book [46]) for the third order Birkhoff normal form Theorem 2.3 in order to give to the reader the feeling about the necessary computations.

Consider a planar analytic map f given by a real power series

$$\begin{aligned} f(x,y) &= (x_1, y_1), \\ x_1 &= \sum_{k=1}^{\infty} \sum_{l=0}^{k} a_{l,k-l}\, x^l y^{k-l}, \\ y_1 &= \sum_{k=1}^{\infty} \sum_{l=0}^{k} b_{l,k-l}\, x^l y^{k-l}, \end{aligned}$$

which converges in a neighbourhood of the origin. Clearly $(x,y) = (0,0)$ is a fixed point of f.

Denote also by $f : \mathbb{C}^2 \to \mathbb{C}^2$ the complex extension of f. Let us assume, that $Df(0)$ has a pair of complex conjugated eigenvalues $\lambda, \overline{\lambda} \in \mathbb{C}$ and denote by $v, \overline{v} \in \mathbb{C}$ their corresponding eigenvectors. Then, using a linear substitution of the form $L = [v^T, \overline{v}^T]$, we can change the coordinate system so that in the new coordinates

$$\begin{aligned} f(\xi,\eta) &= (\lambda\xi + p(\xi,\eta), \bar{\lambda}\eta + q(\xi,\eta)), \\ p(\xi,\eta) &= \sum_{k=2}^{\infty} \sum_{l=0}^{k} p_{l,k-l}\, \xi^l \eta^{k-l}, \\ q(\xi,\eta) &= \sum_{k=2}^{\infty} \sum_{l=0}^{k} q_{l,k-l}\, \xi^l \eta^{k-l}, \\ \overline{p_{i,j}} &= q_{j,i} \qquad \text{for } i,j \geq 0. \end{aligned} \tag{9}$$

The last condition is a consequence of the invariance of $\mathbb{R}^2 \subset \mathbb{C}^2$ under the complex map f. We will refer to it as the *reality condition*. Namely, the set $\mathbb{R}^2 \subset \mathbb{C}^2$ in the new coordinates (ξ,η) is given by $\xi = \overline{\eta}$ and the condition $f(\mathbb{R}^2) \subset \mathbb{R}^2$ expressed in coordinates (ξ,η) is equivalent to Appendix A.

Assume now that $\lambda^k \neq 1$ for $k = 1, \dots, 4$, and consider an analytic area-preserving change of coordinates written as follows

$$\begin{aligned}(\Phi(z,v), \Psi(z,v)) &= (z_1, v_1),\\ z_1 &= z + \sum_{k=2}^{\infty} \sum_{l=0}^{k} \phi_{l,k-l}\, z^l v^{k-l},\\ v_1 &= v + \sum_{k=2}^{\infty} \sum_{l=0}^{k} \psi_{l,k-l}\, z^l v^{k-l},\end{aligned}$$

where the first coefficients are given by

$$\begin{aligned}\overline{\psi_{2,0}} &= \phi_{0,2} = -\lambda^2 p_{0,2}(\lambda^3 - 1)^{-1},\\ \overline{\psi_{1,1}} &= \phi_{1,1} = -p_{1,1}(\lambda - 1)^{-1},\\ \overline{\psi_{0,2}} &= \phi_{2,0} = p_{2,0}(\lambda^2 - \lambda)^{-1},\\ \overline{\psi_{3,0}} &= \phi_{0,3} = -\lambda^3 \left(p_{0,3} + p_{1,1}\phi_{0,2} + 2q_{0,2}\psi_{0,2}\right)(\lambda^4 - 1)^{-1},\\ \overline{\psi_{2,1}} &= \phi_{1,2} = \frac{-\lambda}{\lambda^2 - 1}\left(p_{1,2} + 2p_{2,0}\phi_{0,2} + p_{1,1}\phi_{1,1} + p_{1,1}\psi_{0,2} + 2p_{0,2}\psi_{1,1}\right),\\ \overline{\psi_{1,2}} &= \phi_{2,1} = -\phi_{2,0}\psi_{0,2} + \phi_{0,2}\psi_{2,0},\\ \overline{\psi_{0,3}} &= \phi_{3,0} = \left(p_{3,0} + 2p_{2,0}\phi_{2,0} + p_{1,1}\psi_{2,0}\right)(\lambda^3 - \lambda)^{-1}.\end{aligned}$$

The above substitution also satisfies the reality condition Appendix A and brings $f = (f_1, f_2)$ to the normal form

$$(z,v) \to \big(z(\alpha_0 + \alpha_2 zv), v(\beta_0 + \beta_2 zv)\big) + O((zv)^2)$$

with

$$\begin{aligned}\overline{\beta_0} &= \alpha_0 = \lambda,\\ \overline{\beta_2} &= \alpha_2 = q_{1,2} + 2q_{2,0}\phi_{0,2} + q_{1,1}\phi_{1,1} + q_{1,1}\psi_{0,2} + 2q_{0,2}\psi_{1,1}.\end{aligned}$$

Finally, let $\gamma_0 \in \mathbb{R}$ be such that $\lambda = \alpha_0 = e^{\imath\,\gamma_0}$ (being $\imath$ the imaginary unit). We compute the coefficient γ_1 by

$$\gamma_1 = \frac{-\imath\,\alpha_2}{\alpha_0} = \frac{\imath\,\beta_2}{\beta_0}.$$

From the proof given in [46] it follows that $\gamma_1 \in \mathbb{R}$ and the mapping f in coordinates (z, v) has the form

$$f(z,v) = \left(ze^{\imath\,(\gamma_0 + \gamma_1 zv)}, ve^{-\imath\,(\gamma_0 + \gamma_1 zv)}\right) + O_4,$$

where O_4 is a convergent power series with the terms of degree at least 4.

Again, the coefficients of $f(z,v)$ satisfy the reality condition (9). In order to express this normal form in terms of the real variables we make a linear substitution

$$z = r + \imath\, s, \qquad v = r - \imath\, s.$$

In these coordinates, the mapping f has the form

$$\begin{aligned} f(r,s) &= (r_1, s_1) + O_4, \\ r_1 &= r\cos\left(\gamma_0 + \gamma_1(r^2+s^2)\right) - s\sin\left(\gamma_0 + \gamma_1(r^2+s^2)\right), \\ s_1 &= r\sin\left(\gamma_0 + \gamma_1(r^2+s^2)\right) + s\cos\left(\gamma_0 + \gamma_1(r^2+s^2)\right), \end{aligned}$$

which agrees with Theorem 2.3.

One can derive similar formulas for higher order normal forms. It turns out, however, that when we perform these computations using interval arithmetic [42] we get a strong dependency problem. Therefore, to get thinner enclosures for the coefficients γ_i, $i > 0$ one can numerically solve the system of nonlinear equations by means of the interval Newton method [1, 42, 43].

REFERENCES

[1] G. Alefeld, *Inclusion methods for systems of nonlinear equations - the interval Newton method and modifications*, in Topics in Validated Computations, J. Herzberger, ed., Elsevier Science B.V., 1994, pp. 7–26.

[2] V. I. Arnold, V. V. Kozlov, and A. I. Neishtadt, *Mathematical Aspects of Classical and Celestial Mechanics*, Springer Verlag, 1993.

[3] D. Auerbach, P. Cvitanović, J. Eckmann, G. Gunaratne, and I. Procaccia, *Exploring chaotic motion through periodic orbits*, Phys. Rev. Lett., 58 (1987), pp. 2387–2389.

[4] R. Barrio and F. Blesa, *Systematic search of symmetric periodic orbits in 2DOF Hamiltonian systems*, Chaos, Solitons & Fractals, 41 (2009), pp. 560–582, https://dx.doi.org/10.1016/j.chaos.2008.02.032.

[5] R. Barrio, F. Blesa, and S. Serrano, *Fractal structures in the Hénon-Heiles Hamiltonian*, EPL (Europhysics Letters), 82 (2008).

[6] R. Barrio, F. Blesa, and S. Serrano, *Bifurcations and safe regions in open Hamiltonians*, New J. Phys., 11 (2009), p. 053004 (15pp.).

[7] R. Barrio, F. Blesa, and S. Serrano, *Bifurcations and chaos in Hamiltonian systems*, International Journal of Bifurcation and Chaos, 20 (2010), pp. 1293–1319, https://doi.org/10.1142/S0218127410026496.

[8] R. Barrio, A. Dena, and W. Tucker, *A database of rigorous and high-precision periodic orbits of the Lorenz model*, Computer Physics Communications, 194 (2015), pp. 76–83.

[9] R. Barrio and M. Rodríguez, *Systematic computer assisted proofs of periodic orbits of Hamiltonian systems*, Communications in Nonlinear Science and Numerical Simulation, 19 (2014), pp. 2660–2675.

[10] R. Barrio, M. Rodríguez, and F. Blesa, *Computer-assisted proof of skeletons of periodic orbits*, Computer Physics Communications, 183 (2012), pp. 80–85.

[11] R. Barrio and S. Serrano, *A three-parametric study of the Lorenz model*, Phys. D, 229 (2007), pp. 43–51.

[12] R. Barrio and S. Serrano, *Bounds for the chaotic region in the Lorenz model*, Phys. D, 238 (2009), pp. 1615–1624.

[13] G. D. Birkhoff, *The restricted problem of three bodies*, Rend. Circ. Mat. Palermo, 39 (1915), pp. 265–334.

[14] A. D. Brjuno, *Instability in a Hamiltonian system and the distribution of asteroids*, Mathematics of the USSR-Sbornik, 12 (1970), p. 271.

[15] H. Broer, G. Huitema, and M. Sevryuk, *Quasi-periodicity in families of dynamical systems: order amidst chaos*, vol. 1645 of Lecture Notes in Mathematics, Springer Verlag, 1996.

[16] M. J. Capiński and P. Roldán, *Existence of a center manifold in a practical domain around L_1 in the restricted three-body problem*, SIAM Journal on Applied Dynamical Systems, 11 (2012), pp. 285–318, https://doi.org/10.1137/100810381.
[17] M. J. Capiński and C. Simó, *Computer assisted proof for normally hyperbolic invariant manifolds*, Nonlinearity, 25 (2012), p. 1997.
[18] M. J. Capiński and P. Zgliczyński, *Cone conditions and covering relations for topologically normally hyperbolic invariant manifolds*, Discrete and Continuous Dynamical Systems, 30 (2011), pp. 641–670.
[19] R. Castelli, J.-P. Lessard, and J.D. Mireles James, *Parameterization of invariant manifolds for periodic orbits I: Efficient numerics via the Floquet normal form*, SIAM Journal on Applied Dynamical Systems, 14 (2015), pp. 132–167.
[20] P. Cvitanović, *Invariant measurement of strange sets in terms of cycles*, Phys. Rev. Lett., 61 (1988), pp. 2729–2732.
[21] M. de Aguiar, C. Malta, M. Baranger, and K. Davies, *Bifurcations of periodic trajectories in non-integrable Hamiltonian systems with two degrees of freedom: Numerical and analytical results*, Annals of Physics, 180 (1987), pp. 167–205, https://dx.doi.org/10.1016/0003-4916(87)90044-3.
[22] Á. Dena, A. Abad, and R. Barrio, *Efficient computational approaches to obtain periodic orbits in Hamiltonian systems: application to the motion of a lunar orbiter*, Celestial Mechanics and Dynamical Astronomy, 124 (2016), pp. 51–71, https://doi.org/10.1007/s10569-015-9651-2.
[23] E. Doedel, *AUTO: a program for the automatic bifurcation analysis of autonomous systems*, Congr. Numer., 30 (1981), pp. 265–284.
[24] H. R. Dullin, J. D. Meiss, and D. Sterling, *Generic twistless bifurcations*, Nonlinearity, 13 (2000), p. 203.
[25] F. Dumortier, S. Ibáñez, and H. Kokubu, *New aspects in the unfolding of the nilpotent singularity of codimension three*, Dynam. Syst., 16 (2001), pp. 63–95.
[26] F. Dumortier, S. Ibáñez, and H. Kokubu, *Cocoon bifurcation in three-dimensional reversible vector fields*, Nonlinearity, 19 (2006), p. 305.
[27] S. Farantos, *POMULT: a program for computing periodic orbits in Hamiltonian systems based on multiple shooting algorithms*, J. Comput Phys Commun, 108 (1998), pp. 240–258.
[28] J.-Ll. Figueras and A. Haro, *Reliable Computation of Robust Response Tori on the Verge of Breakdown*, SIAM. J. App. Dyn. Sys. 11(2), 597–628 (2012), http://dx.doi.org/10.1137/100809222.
[29] J.-Ll. Figueras, A. Haro and A. Luque, *Rigorous Computer-Assisted Application of KAM theory: A Modern Approach*, Found. Comp. Math. (2016), 1–71, https://doi.org/10.1007/s10208-016-9339-3.
[30] V. Gelfreich, *Near strongly resonant periodic orbits in a Hamiltonian system*, Proceedings of the National Academy of Sciences, 99 (2002), pp. 13975–13979, https://doi.org/10.1073/pnas.212116699.
[31] M. Hénon and C. Heiles, *The applicability of the third integral of motion: Some numerical experiments*, Astronom. J., 69 (1964), pp. 73–79.
[32] J.D. Mireles James, *Polynomial approximation of one parameter families of (un)stable manifolds with rigorous computer assisted error bounds*, Indagationes Mathematicae, 26 (2015), pp. 225–265.
[33] T. Kapela and C. Simó, *Rigorous KAM results around arbitrary periodic orbits for Hamiltonian systems*, Nonlinearity, 30 (2017), 965–986.
[34] H. Kokubu, D. Wilczak, and P. Zgliczyński, *Rigorous verification of cocoon bifurcations in the Michelson system*, Nonlinearity, 20 (2007), p. 2147.
[35] B. Krauskopf, *Strong resonances and Takens's Utrecht preprint*, in Global Analysis of Dynamical Systems, B. Krauskopf, H. W. Broer, and G. Vegter, eds., Taylor & Francis, 2001, pp. 89–111.
[36] J. Lamb, *Reversing symmetries in dynamical systems*, PhD thesis, Amsterdam University, 1994.
[37] J. S. Lamb, M.-A. Teixeira, and K. N. Webster, *Heteroclinic bifurcations near Hopf-zero bifurcation in reversible vector fields in $\mathbb{R}^3$*, Journal of Differential Equations, 219 (2005), pp. 78–115, https://dx.doi.org/10.1016/j.jde.2005.02.019.
[38] Y.-T. Lau, *The "cocoon" bifurcations in three-dimensional systems with two fixed points*, International Journal of Bifurcation and Chaos, 02 (1992), pp. 543–558, https://doi.org/10.1142/S0218127492000690.
[39] C. K. McCord, *Uniqueness of connecting orbits in the equation $y^{(3)} = y^2 - 1$*, Journal of Mathematical Analysis and Applications, 114 (1986), pp. 584–592, https://doi.org/http://dx.doi.org/10.1016/0022-247X(86)90110-1.

[40] K. R. Meyer, *Generic bifurcation of periodic points*, Trans. Amer. Math. Soc., 149 (1970), pp. 95–107, https://dx.doi.org/10.1090/S0002-9947-1970-0259289-X.
[41] D. Michelson, *Steady solutions of the Kuramoto-Sivashinsky equation*, Physica D: Nonlinear Phenomena, 19 (1986), pp. 89–111, https://dx.doi.org/10.1016/0167-2789(86)90055-2.
[42] R. Moore, *Interval Analysis*, Prentice Hall, Englewood Cliffs, N.J., 1966.
[43] A. Neumeier, *Interval methods for systems of equations*, Cambridge University Press, 1991.
[44] P. Schmelcher and F. K. Diakonos, *Detecting unstable periodic orbits of chaotic dynamical systems*, Phys. Rev. Lett., 78 (1997), pp. 4733–4736.
[45] M. B. Sevryuk, *Reversible systems*, Springer-Verlag, Berlin, 1986.
[46] C. Siegel and J. Moser, *Lectures on Celestial Mechanics*, Springer-Verlag, Berlin Heidelberg New York, 1995.
[47] C. Simó and A. Vieiro, *Resonant zones, inner and outer splittings in generic and low order resonances of area preserving maps*, Nonlinearity, 22 (2009), p. 1191.
[48] M. Tadi, *On computing periodic orbits*, J. Sound Vibration, 283 (2005), pp. 495–506.
[49] D. Viswanath, *The Lindstedt-Poincaré technique as an algorithm for computing periodic orbits*, SIAM Rev., 43 (2001), pp. 478–495.
[50] M. N. Vrahatis, A. E. Periou, V. S. Kalantonis, E. A. Perdios, K. Papadakis, R. Prosmiti, and et al., *Application of the characteristic bisection method for locating and computing periodic orbits in molecular systems.*, J. Comput Phys Commun, 138 (2001), pp. 53–68.
[51] D. Wilczak, `http://www.ii.uj.edu.pl/~wilczak.`
[52] D. Wilczak, *Chaos in the Kuramoto-Sivashinsky equations–a computer-assisted proof*, Journal of Differential Equations, 194 (2003), pp. 433–459, http://dx.doi.org/10.1016/S0022-0396(03)00104-9.
[53] D. Wilczak, *Symmetric heteroclinic connections in the Michelson system: A computer assisted proof*, SIAM Journal on Applied Dynamical Systems, 4 (2005), pp. 489–514, https://doi.org/10.1137/040611112.
[54] D. Wilczak, *The existence of Shilnikov homoclinic orbits in the Michelson system: A computer assisted proof*, Foundations of Computational Mathematics, 6 (2006), pp. 495–535.
[55] D. Wilczak and P. Zgliczyński, *Topological method for symmetric periodic orbits for maps with a reversing symmetry*, Discrete and Continuous Dynamical Systems, 17 (2007), pp. 629–652, https://doi.org/10.3934/dcds.2007.17.629.
[56] D. Wilczak and P. Zgliczyński, *$\mathcal{C}^r$-Lohner algorithm*, Schedae Informaticae, 20 (2011), pp. 9–46, https://doi.org/10.4467/20838476SI.11.001.0287.